1596, 1324 $cm^{-1}$. ESI (+) HRMS (*m/z*): $[M + Na]^+$ calcd for $C_{34}H_{46}N_2O_9S$, 681.2822; found, 681.2812.

**Compound 13d.** Title compound was obtained from **11d** and **12** as described for **13a** in 55% yield after flash-chromatography (1:1 hexanes:EtOAc) as a colorless oil. $^1H$ NMR (500 MHz, $CDCl_3$) $\delta$ 1.24−1.30 (m, 2H), 1.43−1.51 (m, 3H), 1.57−1.63 (m, 1H), 1.96 (q, $J$ = 7 Hz, 2H), 2.80 (dd, $J$ = 10, 14 Hz, 1H), 2.86−2.91 (m, 1H), 3.01 (dd, $J$ = 4.5, 14.5 Hz, 1H), 3.08−3.14 (m, 1H), 3.25−3.30 (m, 2H), 3.40 (dd, $J$ = 8.5, 15 Hz, 1H) 3.58 (br s, 1H), 3.65−3.72 (m, 2H), 3.80−3.82 (m, 2H), 3.87 (s, 3H), 3.88−3.96 (m, 2H), 4.60 (d, $J$ = 5.5 Hz, 2H), 4.90−4.95 (m, 2H), 4.98−5.06 (m, 2H), 5.33 (d, $J$ = 10 Hz, 1H), 5.45 (d, $J$ = 18 Hz, 1H), 5.64 (d, $J$ = 5.5 Hz, 1H), 5.65−5.72 (m, 1H), 6.02−6.10 (m, 1H), 6.47 (d, $J$ = 2 Hz, 1H), 6.53 (dd, $J$ = 2.5, 9 Hz, 1H), 7.17−7.27 (m, 5H), 7.85 (d, $J$ = 9 Hz, 1H). $^{13}C$ NMR (125 MHz, $CDCl_3$) $\delta$ 25.7, 27.8, 33.0, 35.3, 45.2, 49.9, 52.4, 55.0, 55.6, 69.5, 69.9, 70.6, 72.2, 73.3, 100.6, 104.5, 109.2, 114.7, 119.4, 126.4, 128.4, 129.3, 131.9, 133.5, 137.6, 138.1, 155.4, 157.0, 164.7. FT-IR (film, NaCl) $\nu_{max}$ = 3339, 1718, 1594, 1324 $cm^{-1}$. ESI (+) HRMS (*m/z*): $[M + Na]^+$ calcd for $C_{33}H_{44}N_2O_9S$, 667.2665; found, 667.2661.

**Compound 13e.** Title compound was obtained from **11e** and **12** as described for **13a** in 68% yield after flash-chromatography (1:1 hexanes:EtOAc) as a colorless oil. $^1H$ NMR (400 MHz, $CDCl_3$) $\delta$ 1.52−1.61 (m, 3H), 1.81−1.93 (m, 2H), 2.09 (q, $J$ = 7 Hz, 2H), 2.76 (dd, $J$ = 10, 13.7 Hz, 1H), 2.83−2.88 (m, 1H), 3.01 (dd, $J$ = 3.6, 14.2 Hz, 1H), 3.28−3.32 (m, 2H), 3.61−3.69 (m, 2H), 3.78−3.85 (m, 6H), 3.87−3.93 (m, 4H), 4.04 (t, $J$ = 6.5 Hz, 2H), 4.92−5.01 (m, 3H), 5.09−5.16 (m, 3H), 5.60−5.71 (m, 2H), 5.72−5.81 (m, 1H), 6.47−6.51 (m, 2H), 7.14−7.26 (m, 5H), 7.82 (d, $J$ = 8.6 Hz, 1H). $^{13}C$ NMR (100 MHz, $CDCl_3$) $\delta$ 24.9, 25.7, 28.2, 33.2, 35.4, 45.3, 51.0, 52.1, 54.9, 55.7, 69.1, 69.5, 70.7, 71.8, 73.1, 100.3, 104.2, 109.2, 115.0, 119.0, 119.2, 126.3, 128.3, 129.3, 133.4, 133.6, 137.5, 138.0, 155.4, 157.6, 164.8. FT-IR (film, NaCl) $\nu_{max}$ = 3368, 1720, 1596, 1325 $cm^{-1}$. ESI (+) HRMS (*m/z*): $[M + Na]^+$ calcd for $C_{33}H_{44}N_2O_9S$, 667.2665; found, 667.2668.

**Compound 13f.** Title compound was obtained from **11f** and **12** as described for **13a** in 64% yield after flash-chromatography (1:1 hexanes:EtOAc) as a colorless oil. $^1H$ NMR (400 MHz, $CDCl_3$) $\delta$ 1.37−1.43 (m, 1H), 1.54−1.62 (m, 1H), 1.91−1.97 (m, 2H), 2.27 (q, $J$ = 7 Hz, 2H), 2.76 (dd, $J$ = 10.1, 13.9 Hz, 1H), 2.84−2.89 (m, 1H), 3.02 (dd, $J$ = 4, 14.1 Hz, 1H), 3.30−3.37 (m, 2H), 3.54 (br s, 1H), 3.62−3.69 (m, 2H), 3.79−3.87 (m, 5H), 3.88−3.95 (m, 4H), 4.06 (t, $J$ = 6.7 Hz, 2H), 4.96−5.00 (m, 2H), 5.04−5.16 (m, 4H), 5.59−5.67 (m, 2H), 5.76−5.85 (m, 1H), 6.47 (d, $J$ = 1.9 Hz, 1H), 6.50 (dd, $J$ = 2.1, 8.9 Hz, 1H), 7.16−7.26 (m, 5H), 7.82 (d, $J$ = 8.8 Hz, 1H). $^{13}C$ NMR (100 MHz, $CDCl_3$) $\delta$ 25.7, 27.9, 29.7, 35.5, 45.3, 51.0, 52.1, 54.9, 55.7, 68.5, 69.5, 70.7, 71.8, 73.2, 100.3, 104.2, 109.2, 115.7, 119.1, 119.3, 126.4, 128.3, 129.3, 133.5, 137.1, 137.7, 155.4, 157.6, 164.8. FT-IR (film, NaCl) $\nu_{max}$ = 3350, 1720, 1596, 1325 $cm^{-1}$. ESI (+) HRMS (*m/z*): $[M + Na]^+$ calcd for $C_{32}H_{42}N_2O_9S$, 653.2509; found, 653.2509.

**Compound 13g.** Title compound was obtained from **11g** and **12** as described for **13a** in 68% yield after flash-chromatography (1:1 hexanes:EtOAc) as a colorless oil. $^1H$ NMR (400 MHz, $CDCl_3$) $\delta$ 1.39−1.45 (m, 1H), 1.56−1.63 (m, 1H), 1.81 (br s, 1H), 2.61 (q, $J$ = 6.6 Hz, 2H), 2.75−2.80 (m, 1H), 2.86−2.91 (m, 1H), 3.02 (dd, $J$ = 4.1, 14.1 Hz, 1H), 3.32 (d, $J$ = 5.8 Hz, 2H), 3.53 (br s, 1H), 3.64−3.70 (m, 2H), 3.81−3.95 (m, 8H), 4.10 (t, $J$ = 6.7 Hz, 2H), 4.97−5.01 (m, 2H), 5.12−5.20 (m, 4H), 5.62−5.66 (m, 2H), 5.86−5.94 (m, 1H), 6.49 (s, 1H), 6.51 (d, $J$ = 9.1 Hz, 1H), 7.18−7.26 (m, 5H), 7.85 (d, $J$ = 8.8 Hz, 1H). $^{13}C$ NMR (100 MHz, $CDCl_3$) $\delta$ 25.8, 33.2, 35.6, 45.4, 51.2, 52.3, 55.0, 55.8, 68.7, 69.6, 70.8, 71.9, 73.3, 100.5, 104.5, 109.3, 117.9, 119.2, 119.4, 126.5, 128.5, 129.4, 133.5, 133.7, 137.8, 155.4, 157.5, 164.9. FT-IR (film, NaCl) $\nu_{max}$ = 3350, 1722, 1596, 1325 $cm^{-1}$. ESI (+) HRMS (*m/z*): $[M + H]^+$ calcd for $C_{31}H_{40}N_2O_9S$, 617.2533; found, 617.2540.

**Compound 13h.** Title compound was obtained from **11h** and **12** as described for **13a** in 52% yield after flash-chromatography (1:1 hexanes:EtOAc) as a colorless oil. $^1H$ NMR (400 MHz, $CDCl_3$) $\delta$ 1.37−1.43 (m, 1H), 1.54−1.65 (m, 1H), 2.73−2.80 (m, 1H), 2.85−2.90 (m, 1H), 3.02 (dd, $J$ = 2.9, 13.7 Hz, 1H), 3.28−3.39 (m, 2H), 3.51 (br s, 1H), 3.63−3.70 (m, 2H), 3.77−3.95 (m, 10H), 4.62 (d, $J$ = 5.2 Hz, 2H), 4.96−5.06 (m, 2H), 5.10−5.16 (m, 2H), 5.33 (d, $J$ = 10.4 Hz, 1H), 5.45 (d, $J$ = 17.2 Hz, 1H), 5.62−5.66 (m, 2H), 6.01−6.10 (m, 1H), 6.49 (s, 1H), 6.52 (d, $J$ = 8.9 Hz, 1H), 7.18−7.33 (m, 5H), 7.85 (d, $J$ = 8.8 Hz, 1H). $^{13}C$ NMR (100 MHz, $CDCl_3$) $\delta$ 25.7, 35.4, 45.3, 51.4, 52.2, 54.9, 55.7, 69.6, 70.0, 70.7, 71.8, 73.1, 100.7, 104.5, 109.2, 119.1, 119.4, 119.5, 126.4, 128.4, 129.3, 131.8, 133.5, 137.7, 155.3, 157.0, 164.8. FT-IR (film, NaCl) $\nu_{max}$ = 3351, 1717, 1596, 1324 $cm^{-1}$. ESI (+) HRMS (*m/z*): $[M + H]^+$ calcd for $C_{30}H_{38}N_2O_9S$, 603.2376; found, 603.2375.

**Inhibitor 14a.** To stirring solution of **13a** (32 mg, 0.047 mmol) in $CH_2Cl_2$ (15 mL) was added Grubbs' first-generation catalyst (4 mg, 0.0046 mmol). After stirring at 23 °C for 16 h, the solvent was evaporated under reduced pressure and the residue was subjected to flash column chromatography to yield **14a** (27 mg, 88% yield) as a white solid and *E*/*Z* mixture (3:1, determined by HPLC). The isomers were isolated by reverse-phase HPLC using the following conditions: YMC Pack ODS-A column (250 mm × 100 mm, 5 $\mu$m); flow rate = 2.75 mL/min; isocratic 60:40 $CH_3CN$:$H_2O$; $T$ = 35 °C; $\lambda$ = 215 nm; *E* isomer $R_t$ = 16.5 min; *Z* isomer $R_t$ = 14.5 min.

**Compound 14a*E*.** $^1H$ NMR (800 MHz, $CDCl_3$) $\delta$ 1.39−1.44 (m, 2H), 1.48−1.53 (m, 1H), 1.57−1.64 (m, 2H), 1.68−1.74 (m, 3H), 1.77−1.82 (m, 1H), 1.83−1.88 (m, 1H), 1.94−1.98 (m, 1H), 2.10−2,14 (m, 3H), 2.71 (dd, $J$=9.6, 14.1 Hz, 1H), 2.86−2.89 (m, 1H), 2.90 (dd, $J$ = 4.3, 14.1 Hz, 1H), 2.91−2.99 (m, 2H), 3.31−3.33 (m, 1H), 3.61−3.64 (m, 1H), 3.65−3.70 (m, 2H), 3.73 (br s, 1H), 3.76−3.78 (m, 1H), 3.79−3.85 (m, 5H), 3.93 (dd, $J$ = 6.6, 9.4 Hz, 1H), 3.96−3.98 (m, 1H), 4.02−4.05 (m, 1H), 4.87 (d, $J$ = 9.1 Hz, 1H), 4.97−5.00 (m, 1H), 5.44−5.48 (m, 1H), 5.54−5.56 (m, 1H), 5.63 (d, $J$ = 5.1 Hz, 1H), 6.44 (d, $J$ = 2 Hz, 1H), 6.49 (dd, $J$ = 2.2, 8.8 Hz, 1H), 7.13−7.24 (m, 5H), 7.84 (d, $J$ = 8.8 Hz, 1H). $^{13}C$ NMR (125 MHz, $CDCl_3$) $\delta$ 25.1, 25.3, 25.7, 26.8, 29.8, 30.4, 32.5, 35.5, 45.2, 50.6, 51.6, 54.7, 55.6, 68.8, 69.5, 70.7, 71.6, 73.3, 99.9, 103.9, 109.2, 118.1, 126.4, 128.4, 129.3, 130.5, 132.1, 134.0, 137.4, 155.2, 157.9, 164.9. ESI (+) HRMS (*m/z*): $[M+Na]^+$ calcd for $C_{34}H_{46}N_2O_9S$, 681.2822; found, 681.2815.

**Compound 14a*Z*.** $^1H$ NMR (800 MHz, $CDCl_3$) $\delta$ 1.28−1.33 (m, 2H), 1.38−1.47 (m, 2H), 1.52−1.64 (m, 5H), 1.84−1.90 (m, 2H), 2.04−2.08 (m, 2H), 2.16−2.22 (m, 2H), 2.74 (dd, $J$ = 9.5, 14.1 Hz, 1H), 2.88−2.90 (m, 1H), 3.00 (dd, $J$=4.5, 14.1 Hz, 1H), 3.05−3.14 (m, 2H), 3.15 (dd, $J$=9.4, 15.1 Hz, 1H), 3.44−3.48 (m, 1H), 3.61 (br s, 1H), 3.66−3.71 (m, 2H), 3.76−3.89 (m, 6H), 3.95 (dd, $J$ = 6.2, 9.6 Hz, 1H), 4.10−4.15 (m, 1H), 4.87 (d, $J$ = 9.1 Hz, 1H), 5.00−5.03 (m, 1H), 5.35−5.39 (m, 1H), 5.49−5.52 (m, 1H), 5.63 (d, $J$ = 5.2 Hz, 1H), 6.50 (s, 1H), 6.49 (dd, $J$ = 2.3, 8.8 Hz, 1H), 7.17−7.26 (m, 5H), 7.84 (d, $J$=8.8 Hz, 1H). $^{13}C$ NMR (125 MHz, $CDCl_3$) $\delta$ 25.0, 25.1, 25.7, 26.0, 26.6, 27.8, 29.6, 35.5, 45.2, 48.5, 52.0, 54.7, 55.6, 68.8, 69.5, 70.6, 71.9, 73.3, 100.7, 104.2, 109.2, 117.8, 126.4, 128.4, 129.2, 129.8, 130.0, 134.1, 137.5, 155.2, 158.0, 165.0. ESI (+) HRMS (*m/z*): $[M + Na]^+$ calcd for $C_{34}H_{46}N_2O_9S$, 681.2822; found, 681.2819.

**Inhibitor 14b.** The title compound was obtained from a ring closing metathesis reaction of **13b** using Grubbs' first-generation catalyst as described for **14a**. The crude material was purified by silica gel chromatography (60:40 EtOAc:hexanes) to give the desired product (50% yield) as a mix of *E*/*Z* isomers (27:73 by HPLC). The isomers were isolated by chiral HPLC using the following conditions: Chiralpak IA column (250 mm × 4.6 mm, 5 $\mu$m); flow rate = 0.75 mL/min; isocratic 60:40 IPA: hexanes; $T$=25 °C; $\lambda$=215 nm; *E* isomer $R_t$=7.56 min; *Z*-isomer $R_t$ = 8.89 min.

**Compound 14b*E*.** $^1H$ NMR (800 MHz, $CDCl_3$) $\delta$ 1.60−1.20 (m, 4H), 2.30−1.90 (m, 7H), 3.10−2.80 (m, 5H), 3.32 (m, 1H),

4.00−3.50 (m, 12 H), 4.15 (m, 2H), 4.98 (m, 2H), 5.45 (m, 1H), 5.63 (m, 2H), 6.51 (m, 2H), 7.25−7.15 (m, 5H), 7.76 (d, $J$ = 19.2 Hz, 1H). $^{13}$C NMR (125 MHz, $CDCl_3$) $\delta$ 23.1, 24.8, 25.0, 25.7, 26.2, 26.6, 29.0, 35.5, 45.2, 48.2, 52.0, 54.8, 55.6, 67.1, 69.5, 70.7, 71.6, 73.3, 100.1, 104.0, 109.2, 114.6, 118.4, 126.4, 128.4, 128.9, 129.3, 130.6, 133.8, 137.4, 155.3, 157.7, 164.9.; ESI (+) HRMS ($m/z$): $[M + Na]^+$ calcd for $C_{33}H_{44}N_2O_9S$, 667.2665; found, 667.2660.

**Compound 14b*Z*.** $^1$H NMR (800 MHz, $CDCl_3$) $\delta$ 1.60−1.0 (m, 7H), 1.72 (m, 2H), 1.90 (m, 3H), 2.21 (m, 2H), 2.43 (m, 1H), 2.55 (m, 1H), 2.67 (m, 1H), 2.76 (m, 1H), 2.84 (m, 1H), 3.01 (m, 1H), 3.26 (m, 1H), 3.41 (m, 3H), 3.60 (m, 4H), 3.69 (m, 1H), 3.86 (m, 2H), 4.43 (d, $J$ = 15.2 Hz, 1H), 4.83 (m, 1H), 5.24 (m, 1H), 5.33 (m, 1H), 5.51 (d, $J$=8.8 Hz, 1H), 6.45 (m, 2H), 7.17 (m, 3H), 7.24 (m, 2H), 7.87 (d, $J$=13.6 Hz, 1H). $^{13}$C NMR (125 MHz, $CDCl_3$) $\delta$ 24.7, 25.7, 27.3, 28.6, 30.9, 32.1, 35.5, 45.2, 49.3, 51.8, 54.8, 55.6, 69.5, 70.7, 71.0, 71.9, 73.3, 101.2, 104.3, 109.2, 119.3, 126.4, 128.4, 128.9, 129.3, 130.8, 130.9, 133.4, 137.5, 155.3, 158.2, 164.5. ESI (+) HRMS ($m/z$): $[M+Na]^+$ calcd for $C_{33}H_{44}N_2O_9S$, 667.2665; found, 667.2667.

**Inhibitor 14c.** Title compound was obtained from **13c** and Grubbs' first-generation catalyst as described for **14a** in 89% yield after flash-chromatography (2:3 hexanes:EtOAc) as a white solid and $E/Z$ mixture (3:1, determined by HPLC). The isomers were isolated using reversed-phase HPLC under the following conditions: YMC Pack ODS-A column (250 mm × 100 mm, 5 $\mu$m); flow rate = 2.75 mL/min; isocratic 60:40 $CH_3CN$:$H_2O$; $T$ = 35 °C; $\lambda$ = 215 nm; $E$ isomer $R_t$ = 13.43 min; $Z$ isomer $R_t$ = 11.76 min.

**Compound 14c*E*.** $^1$H NMR (800 MHz, $CDCl_3$) $\delta$ 1.45−1.54 (m, 3H), 1.56−1.64 (m, 2H), 1.68−1.72 (m, 1H), 2.11−2.20 (m, 2H), 2.52−2.62 (m, 2H), 2.79 (dd, $J$=9.6, 14 Hz, 1H), 2.87−2.90 (m, 1H), 2.96−3.00 (m, 2H), 3.04 (dd, $J$ = 4.2, 14.2 Hz, 1H), 3.40−3.44 (m, 1H), 3.53−3.56 (m, 1H), 3.66−3.70 (m, 3H), 3.82−3.89 (m, 6H), 3.94 (dd, $J$ = 6.3, 9.5 Hz, 1H), 4.07−4.14 (m, 2H), 4.96 (d, $J$ = 9.4 Hz, 1H), 4.98−5.01 (m, 1H), 5.53−5.56 (m, 1H), 5.64−5.68 (m, 2H), 6.52−6.53 (m, 2H), 7.18−7.27 (m, 5H), 7.76 (d, $J$ = 9.4 Hz, 1H). $^{13}$C NMR (125 MHz, $CDCl_3$) $\delta$ 24.4, 25.7, 28.3, 32.3, 32.4, 35.6, 45.2, 49.6, 51.9, 54.9, 55.6, 69.5, 69.9, 70.7, 71.9, 73.2, 101.9, 104.9, 109.2, 119.3, 126.4, 128.0, 128.4, 129.3, 133.4, 133.9, 137.6, 155.3, 158.0, 164.5. ESI (+) HRMS ($m/z$): $[M + H]^+$ calcd for $C_{32}H_{42}N_2O_9S$, 631.2689; found, 631.2698.

**Compound 14c*Z*.** $^1$H NMR (500 MHz, $CDCl_3$) $\delta$ 1.48−1.52 (m, 3H), 1.57−1.72 (m, 3H), 2.10−2.14 (m, 1H), 2.28−2.32 (m, 1H), 2.47−2.51 (m, 1H), 2.78 (dd, $J$ = 9, 14 Hz, 2H), 2.87−2.91 (m, 1H), 2.98−3.08 (m, 3H), 3.45−3.60 (m, 2H), 3.65−3.71 (m, 3H), 3.80−3.90 (m, 6H), 3.95 (dd, $J$ = 6, 9.5 Hz, 1H), 4.07−4.10 (m, 1H), 4.18−4.21 (m, 1H), 4.95 (d, $J$ = 9.5 Hz, 1H), 4.98−5.02 (m, 1H), 5.44−5.49 (m, 2H), 5.63 (d, $J$ = 5.5 Hz, 1H), 6.51 (dd, $J$ = 2.5, 9.8 Hz, 1H), 6.53 (d, $J$ = 2 Hz, 1H), 7.18−7.27 (m, 5H), 7.81 (d, $J$=9 Hz, 1H). $^{13}$C NMR (125 MHz, $CDCl_3$) $\delta$ 24.7, 24.8, 25.7, 26.3, 27.7, 35.5, 45.2, 46.9, 50.2, 54.9, 55.6, 69.5, 69.9, 70.6, 70.7, 73.2, 101.9, 104.8, 109.1, 120.5, 126.4, 127.6, 128.4, 129.3, 129.6, 132.5, 133.2, 137.6, 155.3, 158.1, 164.6. ESI (+) HRMS ($m/z$): $[M + H]^+$ calcd for $C_{32}H_{42}N_2O_9S$, 631.2689; found, 631.2706.

**Inhibitor 14d.** Title compound was obtained from **13d** and Grubbs' first-generation catalyst as described for **14a** in 71% yield after flash-chromatography (2:3 hexanes:EtOAc) as a white solid. $^1$H NMR (500 MHz, $CDCl_3$) $\delta$ 1.40−1.47 (m, 1H), 1.58−1.62 (m, 2H), 1.92−1.95 (m, 1H), 2.11−2.15 (m, 1H), 2.28−2.39 (m, 2H), 2.73−2.78 (m, 1H), 2.80−3.05 (m, 6H), 3.64−3.70 (m, 3H), 3.80−3.89 (m, 6H), 3.93−3.96 (m, 2H), 4.12−4.15 (m, 1H), 4.62 (br s, 1H), 4.97−4.99 (m, 1H), 5.11 (d, $J$ = 9.2 Hz, 1H), 5.52−5.54 (m, 2H), 5.61 (d, $J$ = 5.1 Hz, 1H), 6.46−6.49 (m, 2H), 7.18−7.26 (m, 5H), 7.80 (d, $J$ = 9.4 Hz, 1H). $^{13}$C NMR (125 MHz, $CDCl_3$) $\delta$ 22.6, 22.9, 23.4, 25.7, 25.9, 29.6, 35.4, 45.1, 45.2, 47.9, 55.0, 55.6, 62.0, 69.5, 70.7, 73.2, 100.2, 103.6, 109.2, 119.9, 123.5, 126.4, 128.4, 129.3, 132.6, 137.6, 140.4, 155.4, 156.4, 164.3. ESI (+) HRMS ($m/z$): $[M + H]^+$ calcd for $C_{31}H_{40}N_2O_9S$, 617.2533; found, 617.2534.

**Inhibitor 14e.** Title compound was obtained from **13e** and Grubbs' second-generation catalyst as described for **14a** in 52% yield after flash-chromatography (2:3 hexanes:EtOAc) as a white solid. $^1$H NMR (500 MHz, $CDCl_3$) $\delta$ 1.46−1.51 (m, 1H), 1.60−1.76 (m, 4H), 1.88−1.92 (m, 2H), 2.23−2.37 (m, 2H), 2.79 (dd, $J$=9, 14 Hz, 1H), 2.88−3.01 (m, 2H), 3.10−3.13 (m, 2H), 3.57 (br s, 1H), 3.66−3.72 (m, 2H), 3.72−3.89 (m, 5H), 3.92−3.99 (m, 2H), 4.07−4.15 (m, 2H), 4.94 (d, $J$ = 8.5 Hz, 1H), 5.00−5.04 (m, 1H), 5.44−5.54 (m, 3H), 5.64 (d, $J$ = 5.1 Hz, 1H), 6.43 (d, $J$ = 2 Hz, 1H), 6.49−6.51 (m, 1H), 7.16−7.28 (m, 5H), 7.81 (d, $J$=9 Hz, 1H). $^{13}$C NMR (125 MHz, $CDCl_3$) $\delta$ 25.7, 26.3, 26.5, 27.4, 29.6, 35.5, 43.9, 45.2, 50.7, 54.7, 55.6, 69.5, 69.7, 70.7, 73.3, 100.0, 103.9, 109.2, 117.7, 122.9, 126.4, 128.4, 129.3, 133.7, 135.1, 137.4, 155.3, 157.7, 164.9. ESI (+) HRMS ($m/z$): $[M + Na]^+$ calcd for $C_{31}H_{40}N_2O_9S$, 639.2352; found, 639.2345.

**Inhibitor 14f.** Title compound was obtained from **13f** and Grubbs' second-generation catalyst as described for **14a** in 81% yield after flash-chromatography (2:3 hexanes:EtOAc) as a white solid. $^1$H NMR (500 MHz, $CDCl_3$) $\delta$ 1.40−1.47 (m, 1H), 1.58−1.62 (m, 2H), 1.92−1.95 (m, 1H), 2.11−2.15 (m, 1H), 2.28−2.39 (m, 2H), 2.73−2.78 (m, 1H), 2.80−3.05 (m, 5H), 3.64−3.70 (m, 2H), 3.80−3.89 (m, 6H), 3.93−3.96 (m, 2H), 4.12−4.15 (m, 1H), 4.62 (br s, 1H), 4.97−4.99 (m, 1H), 5.11 (d, $J$ = 9.2 Hz, 1H), 5.52−5.54 (m, 2H), 5.61 (d, $J$ = 5.1 Hz, 1H), 6.46−6.49 (m, 2H), 7.18−7.26 (m, 5H), 7.80 (d, $J$ = 9.4 Hz, 1H). $^{13}$C NMR (125 MHz, $CDCl_3$) $\delta$ 22.7, 25.1, 25.7, 29.6, 35.5, 41.2, 45.3, 47.8, 54.8, 55.6, 65.9, 69.5, 70.7, 73.2, 101.0, 104.3, 109.2, 118.7, 123.3, 126.4, 128.4, 129.3, 133.4, 133.6, 137.5, 155.4, 157.8, 164.7. ESI (+) HRMS ($m/z$): $[M + H]^+$ calcd for $C_{30}H_{38}N_2O_9S$, 603.2376; found, 603.2369.

**Inhibitor 14g.** Title compound was obtained from **13g** and Grubbs' second-generation catalyst as described for **14a** in 81% yield after flash-chromatography (2:3 hexanes:EtOAc) as a white solid. $^1$H NMR (500 MHz, $CDCl_3$) $\delta$ 1.47−1.55 (m, 1H), 1.64−1.70 (m, 2H), 2.51−2.54 (m, 1H), 2.73−2.78 (m, 1H), 2.84−3.94 (m, 2H), 3.04−3.11 (m, 2H), 3.19 (d, $J$=13.6 Hz, 1H), 3.70−3.75 (m, 2H), 3.86 (s, 4H), 3.94−3.99 (m, 4H), 4.07−4.08 (m, 1H), 4.18 (br s, 1H), 4.58 (s, 1H), 5.02−5.06 (m, 1H), 5.12 (s, 1H), 5.61 (d, $J$ = 5 Hz, 1H), 5.76−5.82 (m, 1H), 5.88−5.93 (m, 1H), 6.35 (d, $J$=1.1 Hz, 1H), 6.51 (dd, $J$ = 1.5, 8.7 Hz, 1H), 7.20−7.31 (m, 5H), 7.79 (d, $J$ = 8.8 Hz, 1H). $^{13}$C NMR (125 MHz, $CDCl_3$) $\delta$ 25.8, 26.7, 35.4, 43.6, 45.3, 47.1, 55.1, 55.7, 67.4, 69.6, 70.5, 70.8, 73.3, 99.4, 104.1, 109.2, 120.5, 126.5, 126.9, 128.5, 129.4, 131.2, 132.0, 137.6, 155.6, 157.4, 164.7. ESI (+) HRMS ($m/z$): $[M + Na]^+$ calcd for $C_{29}H_{36}N_2O_9S$, 611.2039; found, 611.2040.

**Inhibitor 14h.** Title compound was obtained from **13h** and Grubbs' second-generation catalyst as described for **14a** in 79% yield after flash-chromatography (2:3 hexanes:EtOAc) as a white solid. $^1$H NMR (400 MHz, $CDCl_3$) $\delta$ 1.45−1.51 (m, 1H), 1.60−1.68 (m, 2H), 2.80−2.90 (m, 2H), 3.00−3.12 (m, 3H), 3.53 (br s, 1H), 3.66−3.71 (m, 2H), 3.83 (s, 4H), 3.92−3.95 (m, 3H), 4.25 (br s, 1H), 4.88−5.01 (m, 3H), 5.13 (d, $J$ = 8.3 Hz, 1H), 5.63 (d, $J$ = 5.1 Hz, 1H), 5.72−5.76 (m, 2H), 6.59−6.64 (m, 2H), 7.19−7.26 (m, 5H), 7.74 (d, $J$=8.7 Hz, 1H). $^{13}$C NMR (125 MHz, $CDCl_3$) $\delta$ 25.7, 29.6, 35.3, 43.9, 45.2, 47.8, 55.1, 55.7, 69.5, 70.7, 71.1, 73.3, 104.5, 107.2, 109.2, 123.4, 126.1, 126.4, 128.4, 129.3, 131.3, 131.5, 137.6, 155.6, 157.7, 164.5. ESI (+) HRMS ($m/z$): $[M + Na]^+$ calcd for $C_{28}H_{34}N_2O_9S$, 597.1883; found, 597.1887.

**Inhibitor 15a.** To a stirring solution of **14a** (10 mg, 0.015 mmol) in EtOAc (2 mL) was added 10% Pd on carbon and the reaction was stirred under $H_2$ atmosphere for 12 h. After this time, the reaction was filtered through a pad of celite and solvent was evaporated under reduced pressure. The residue was then purified by flash-chromatography to give **15a** (9 mg, 93% yield) as a white solid. $^1$H NMR (500 MHz, $CDCl_3$) $\delta$ 0.87−0.92 (m, 2H), 1.25−1.28 (m, 8H), 1.38−1.49 (m, 5H), 1.60−1.64 (m, 3H),

1.71−1.83 (m, 4H), 2.32−2.38 (m, 1H), 2.75 (dd, $J$ = 9.5, 13.7 Hz, 1H), 2.86−2.91 (m, 1H), 3.01−3.10 (m, 3H), 3.64−3.71 (m, 2H), 3.85 (s, 4H), 3.94 (dd, $J$ = 6.4, 9.5 Hz, 1H), 4.01−4.04 (m, 1H), 4.10−4.16 (m,1H), 4.94 (d, $J$ = 9.2 Hz, 1H), 5.01−5.15 (m, 1H), 5.67 (d, $J$ = 5.1 Hz, 1H), 6.52−6.54 (m, 2H), 7.19−7.29 (m, 5H), 7.85 (d, $J$ = 9 Hz, 1H). $^{13}$C NMR (125 MHz, $CDCl_3$) $\delta$ 23.8, 24.2, 25.5, 26.3, 26.4, 28.2, 29.1, 29.4, 35.3, 45.1, 51.3, 52.8, 54.6, 55.4, 69.2, 69.3, 69.5, 70.5, 71.9, 73.1, 100.2, 103.9, 109.0, 118.7, 126.3, 128.2, 129.1, 133.5, 137.3, 155.1, 157.9, 164.6. ESI (+) HRMS ($m/z$): $[M + Na]^+$ calcd for $C_{34}H_{48}N_2O_9S$, 683.2978; found, 683.2984.

**Inhibitor 15b.** Title compound was obtained from **14b** as described for **15a** in 90% yield after flash-chromatography (2:3 hexanes:EtOAc) as a white solid. $^1$H NMR (500 MHz, $CDCl_3$) $\delta$ 1.30−1.47 (m, 8H), 1.57−1.70 (m, 5H), 1.72−1.79 (m, 1H), 1.82−1.87 (m, 2), 2.77 (dd, $J$ = 10, 14 Hz, 1H), 2.86−2.91 (m, 1H),3.00 (dd, $J$ = 4.5, 14 Hz, 1H), 3.05 (d, $J$ = 2.5, 15 Hz, 1H), 3.14−3.23 (m, 2H), 3.56−3.62 (m, 2H), 3.65−3.72 (m, 2H), 3.81−3.90 (m, 6H), 3.94 (dd, $J$ = 6.5, 10 Hz, 1H), 4.05−4.15 (m, 2H), 4.96 (d, $J$ = 9.5 Hz, 1H), 4.99−5.02 (m, 1H), 5.64 (d, $J$ = 5.5 Hz, 1H), 6.49−6.52 (m, 2H), 7.17−7.27 (m, 5H), 7.82 (d, $J$ = 9.5 Hz, 1H). $^{13}$C NMR (125 MHz, $CDCl_3$) $\delta$ 23.2, 24.2, 24.9, 25.2, 25.7, 26.1, 27.6, 28.9, 35.4, 45.2, 49.2, 52.7, 54.8, 55.6, 68.9, 69.5, 70.7, 71.7, 73.2, 100.5, 104.2, 109.2, 118.5, 126.4, 128.4, 129.3, 133.8, 137.5, 155.3, 158.1, 164.8. ESI (+) HRMS ($m/z$): $[M + Na]^+$ calcd for $C_{33}H_{46}N_2O_9S$, 669.2822; found, 669.2828.

**Inhibitor 15c.** Title compound was obtained from **14c** as described for **15a** in 90% yield after flash-chromatography (2:3 hexanes:EtOAc) as a white solid. $^1$H NMR (500 MHz, $CDCl_3$) $\delta$ 1.35−1.39 (m, 3H), 1.40−1.54 (m, 4H), 1.60−1.66 (m, 6H), 1.85−1.98 (m, 2H), 2.78 (dd, $J$=9.1, 14 Hz, 1H), 2.88−2.91 (m, 1H),2.97−3.03 (m, 1H), 3.06−3.14 (m, 1H), 3.39−3.43 (m, 1H), 3.50−3.56 (m, 1H), 3.66−3.72 (m, 3H), 3.82−3.85 (m, 6H), 3.95 (dd, $J$ = 6.3, 9.6 Hz, 1H), 4.07−4.10 (m, 2H), 4.95−5.03 (m, 2H), 5.64 (d, $J$ = 5 Hz, 1H), 6.50−6.53 (m, 2H), 7.17−7.27 (m, 5H), 7.82 (d, $J$=9 Hz, 1H). $^{13}$C NMR (125 MHz, $CDCl_3$) $\delta$ 22.6, 23.5, 24.0, 24.6, 25.3, 25.7, 26.1, 35.5, 44.8, 45.2, 46.5, 51.0, 54.8, 55.6, 69.5, 70.1, 70.7, 70.8, 73.2, 100.9, 104.3, 109.2, 118.5, 126.4, 128.4, 129.4, 133.9, 137.5, 155.2, 158.2, 164.8. ESI (+) HRMS ($m/z$): $[M + Na]^+$ calcd for $C_{32}H_{44}N_2O_9S$, 655.2668; found, 655.2667.

**Inhibitor 15d.** Title compound was obtained from **14d** or **14e** as described for **15a** in 94% yield after flash-chromatography (2:3 hexanes:EtOAc) as a white solid. $^1$H NMR (500 MHz, $CDCl_3$) $\delta$ 1.33−1.54 (m, 6H), 1.57−1.74 (m, 3H), 1.86−1.94 (m, 2H), 2.77 (dd, $J$=9.5, 14 Hz, 1H), 2.86−2.90 (m, 1H), 2.96−3.08 (m, 3H), 3.24−3.29 (m, 1H), 3.64−3.72 (m, 2H), 3.74−3.86 (m, 7H), 3.94−4.00 (m, 2H), 4.15−4.22 (m, 2H), 4.92 (d, $J$ = 9.2 Hz, 1H), 4.97−5.02 (m, 1H), 5.62 (d, $J$ = 5.2 Hz, 1H), 6.48 (d, $J$=2.1 Hz, 1H), 6.52 (dd, $J$=2, 8.9 Hz, 1H), 7.17−7.27 (m, 5H), 7.87 (d, $J$ = 8.6 Hz, 1H) $^{13}$C NMR (125 MHz, $CDCl_3$) $\delta$ 23.2, 25.0, 25.6, 26.1, 26.3, 35.4, 42.9, 45.2, 48.5, 54.7, 55.6, 69.3, 69.5, 70.7, 73.3, 99.9, 103.8, 109.1, 117.1, 126.4, 128.4, 129.3, 134.6, 137.4, 155.1, 157.7, 165.2. ESI (+) HRMS ($m/z$): $[M + Na]^+$ calcd for $C_{31}H_{42}N_2O_9S$, 641.2509; found, 641.2512.

**Inhibitor 15f.** Title compound was obtained from **14f** as described for **15a** in 93% yield after flash-chromatography (2:3 hexanes:EtOAc) as a white solid. $^1$H NMR (500 MHz, $CDCl_3$) $\delta$ 1.33−1.48 (m, 4H), 1.56−1.66 (m, 3H), 1.67−1.71 (m, 2H), 1.83−1.86 (m, 1H), 2.04−2.12 (m, 2H), 2.74 (dd, $J$ = 9.7, 14 Hz, 1H), 2.83−2.99 (m, 4H), 3.18 (br s, 1H), 3.64−3.71 (m, 2H), 3.76−3.85 (m, 6H), 3.89−3.99 (m, 3H), 4.08 (br s, 1H), 4.19−4.23 (m, 1H), 4.96−5.00 (m, 2H), 5.63 (d, $J$ = 5 Hz, 1H), 6.45 (d, $J$ = 2 Hz, 1H), 6.50 (dd, $J$ = 2.5, 9 Hz, 1H), 7.15−7.26 (m, 5H), 7.88 (d, $J$=9 Hz, 1H). $^{13}$C NMR (125 MHz, $CDCl_3$) $\delta$ 22.2, 24.4, 24.6, 25.7, 25.8, 35.4, 45.2, 46.8, 51.8, 54.7, 55.7, 69.2, 69.6, 70.5, 70.8, 73.3, 99.8, 103.9, 109.2, 117.5, 126.5, 128.4, 129.3, 134.3, 137.4, 155.2, 157.8, 165.3. ESI (+) HRMS ($m/z$): $[M + Na]^+$ calcd for $C_{30}H_{40}N_2O_9S$, 605.2533; found, 605.2526.

**Inhibitor 15g.** Title compound was obtained from **14g** as described for **15a** in 90% yield after flash-chromatography (2:3 hexanes:EtOAc) as a white solid. $^1$H NMR (500 MHz, $CDCl_3$) $\delta$ 1.46−1.50 (m, 3H), 1.59−1.67 (m, 4H), 1.96−2.04 (m, 2H), 2.81−2.91 (m, 2H), 3.03 (dd, $J$ = 3, 14 Hz, 1H), 3.07−3.12 (m, 2H), 3.56 (br s, 1H), 3.57−3.71 (m, 2H), 3.83−3.91 (m, 6H), 3.93−4.02 (m, 3H), 4.25 (br s, 1H), 4.98−5.02 (m, 2H), 5.63 (d, $J$ = 5 Hz, 1H), 6.40 (d, $J$ = 2 Hz, 1H), 6.49 (dd, $J$ = 2, 9 Hz, 1H), 7.18−7.28 (m, 5H), 7.76 (d, $J$ = 9 Hz, 1H). $^{13}$C NMR (125 MHz, $CDCl_3$): $\delta$ 22.4, 24.4, 25.3, 25.7, 35.4, 43.1, 45.2, 47.3, 54.9, 55.6, 69.5, 70.1, 70.6, 70.7, 73.2, 100.5, 104.2, 109.2, 121.4, 126.4, 128.4, 129.3, 131.5, 137.5, 155.4, 157.7, 164.5. ESI (+) HRMS ($m/z$): $[M + H]^+$ calcd for $C_{29}H_{38}N_2O_9S$, 591.2376; found, 591.2381.

**Inhibitor 15h.** Title compound was obtained from **14h** as described for **15a** in 92% yield after flash-chromatography (2:3 hexanes:EtOAc) as a white solid. $^1$H NMR (500 MHz, $CDCl_3$) $\delta$ 1.39−1.51 (m, 3H), 1.60−1.68 (m, 3H), 1.72−1.81 (m, 2H), 2.82−2.92 (m, 2H), 3.00−3.06 (m, 3H), 3.66−3.71 (m, 3H), 3.80−3.87 (m, 6H), 3.95 (dd, $J$=6, 9.5 Hz, 1H), 3.97−4.02 (m, 1H), 4.25 (br s, 1H), 4.98−5.02 (m, 2H), 5.63 (d, $J$ = 5 Hz, 1H), 6.62−6.64 (m, 2 H), 7.18−7.28 (m, 5H), 7.77 (d, $J$=10.5 Hz, 1H). $^{13}$C NMR (125 MHz, $CDCl_3$) $\delta$ 24.3, 25.0, 25.7, 35.3, 44.5, 45.2, 46.5, 55.0, 55.6, 69.5, 70.6, 73.2, 73.9, 105.6, 107.3, 109.1, 126.4, 128.4, 129.3, 130.9, 137.3, 155.5, 157.4, 164.4. ESI (+) HRMS ($m/z$): $[M + H]^+$ calcd for $C_{28}H_{36}N_2O_9S$, 577.2220; found, 577.2222.

***tert*-Butyl-(2*S*,3*R*)-4-(2,2-dimethylpent-4-enylamino)-3-hydroxy-1-phenylbutan-2-ylcarbamate (17a).** A stirring solution of amine **16a** (1.58 g, 4.33 mmol) and epoxide **8** (304 mg, 1.15 mmol) was heated to 60 °C for 4 h and allowed to stir at 23 °C overnight. The reaction mixture was concentrated and purified by silica chromatography (3:97 MeOH:$CH_2Cl_2$) to give 370 mg (98% yield) of product as a clear oil that solidified upon refrigeration. $[\alpha]_D^{20}$ +0.9 ($c$ 0.14, $CHCl_3$). $^1$H NMR ($CDCl_3$, 400 MHz) $\delta$ 0.90 (s, 6H), 1.36 (s, 9H), 2.01 (d, $J$ = 7.6 Hz, 2H), 2.35 (s, 2H), 2.69 (d, $J$ = 4.8 Hz, 2H), 2.87 (dd, $J$ = 8, 14.8 Hz, 1H), 2.98 (dd, $J$ = 4.8, 9.2 Hz, 1H), 3.45 (m, 1H), 3.82 (m, 1H), 4.79 (d, $J$ = 9.2 Hz, 1H), 5.03 (m, 2H), 5.81 (m, 1H), 7.26 (m, 5H). $^{13}$C NMR ($CDCl_3$, 100 MHz) $\delta$ 25.4, 25.4, 29.6, 34.3, 36.8, 44.5, 52.1, 54.3, 60.1, 70.3, 79.1, 116.9, 126.2, 128.3, 129.4, 135.2, 137.9, 155.8. FTIR (NaCl) $\nu_{max}$ = 3349, 3064, 2928, 1693, 1391, 1366, cm$^{-1}$. ESI LRMS ($m/z$): 376.06 $[M + H]^+$.

***tert*-Butyl-(2*S*,3*R*)-4-(*N*-(2,2-dimethylpent-4-enyl)-2-(hex-5-enyloxy)-4-methoxyphenylsulfonamido)-3-hydroxy-1-phenylbutan-2-ylcarbamate (18a).** To a mixture of amine **17a** (188 mg, 0.5 mmol) and sulfonyl chloride **7d** (183 mg, 0.6 mmol) at 0 °C under argon atmosphere was added pyridine (8 mL, freshly distilled over KOH), and the reaction was allowed to warm to 23 °C while stirring. The reaction turned orange and was allowed to stir overnight. The reaction was condensed under reduced pressure, washed with saturated $CuSO_4$, and the product extracted with dichloromethane. The organic layer was washed with $H_2O$, brine, dried over sodium sulfate, and purified by silica chromatography (20:80 EtOAc:hexanes) to give **18a** (180 mg, 56% yield) as a clear oil. $[\alpha]_D^{20}$ +18.3 ($c$ 0.12, $CHCl_3$). $^1$H NMR ($CDCl_3$, 400 MHz) $\delta$ 0.90 (s, 3H), 0.92 (s, 3H), 1.25 (m, 1H), 1.31 (s, 9H), 1.59 (m, 2H), 1.86 (quintet, $J$ = 8 Hz, 2H), 1.99 (d, $J$ = 7.2 Hz, 2H), 2.12 (q, $J$ = 6.8 Hz, 2H), 2.77 (dd, $J$=8, 13.2 Hz, 1H), 2.86 (dd, $J$ = 4.8, 14.4 Hz, 1H), 3.20 (m, 4H), 3.66 (m, 1H), 3.80 (m, 1H), 3.83 (s, 3H), 4.00 (m, 2H), 4.40 (d, $J$ = 8.8 Hz, 1H), 5.00 (m, 4H), 5.79 (m, 2H), 6.47 (m, 2H), 7.20 (m, 5H),7.78 (d, $J$ = 8.4 Hz, 1H). $^{13}$C NMR ($CDCl_3$, 100 MHz) $\delta$ 25.0, 25.5, 25.6, 28.0, 28,2, 28.4, 33.2, 35.8, 45.2, 54.2, 55.5, 55.6, 62.4, 69.1, 72.0, 79.3, 100.1, 104.2, 115.1, 117.5, 118.5, 126.2, 128.3, 129.4, 134.0, 134.7, 137.6, 138.0, 155.5, 157.5, 164.8. FTIR (NaCl) $\nu_{max}$=3412, 2852, 1701, 1596, 1496, 1456, 1391, 1367 cm$^{-1}$. ESI (+) HRMS ($m/z$): $[M + Na^+]$ calcd for $C_{35}H_{52}N_2O_7S$ 667.3393; found, 667.3399.

**(3*R*,3a*S*,6a*R*)-Hexahydrofuro[2,3-*b*]furan-3-yl (2*S*,3*R*)-4-(*N*-(2,2-Dimethylpent-4-enyl)-2-(hex-5-enyloxy)-4-methoxyphenylsulfonamido)-3-hydroxy-1-phenylbutan-2-ylcarbamate (19a).** To a stirring

solution of **18a** (180 mg, 0.28 mmol) in $CH_2Cl_2$ (5 mL) at 0 °C was added trifluoroacetic acid (1.5 mL). The reaction was allowed to warm to 23 °C and stirred overnight. Solvents were removed under reduced pressure, and saturated aqueous $NaHCO_3$ and 1N NaOH (1 mL) was added and extracted with ether. Solvents were removed under reduced pressure to afford the crude amine product.

To a solution of above amine (0.28 mmol) in MeCN (20 mL) was added carbonate **12** (92 mg, 0.31 mmol) under argon followed by dropwise addition of *i*-$Pr_2NEt$ (1 mL) and pyridine (1 mL), and the reaction was allowed to stir overnight at 23 °C. After stirring for 2 days, the solvent was removed under reduced pressure and the crude material purified by silica gel column chromatography (50:50 EtOAc:hexanes) to give **19a** (144 mg, 73% yield over two steps) as a white solid; mp = 49−52 °C; $[\alpha]_D^{20}$ +3.9 (*c* 1.03, $CHCl_3$). $^1$H NMR ($CDCl_3$, 400 MHz) $\delta$ 0.90 (s, 3H), 0.91 (s, 3H), 1.35 (m, 1H), 1.58 (m, 3H), 1.86 (m, 2H), 2.02 (m, 3H), 2.11 (m, 2H), 2.69 (dd, $J$ = 9.6, 14 Hz, 1H), 2.84 (m, 1H), 2.94 (dd, $J$ = 4, 14.4 Hz, 1H), 3.08 (m, 2H), 3.29 (m, 2H), 3.63 (m, 2H), 3.78 (m, 2H), 3.83 (s, 3H), 3.91 (m, 3H), 4.03 (m, 2H), 4.87 (d, $J$ = 9.6 Hz, 1H), 5.02 (m, 4H), 5.60 (d, $J$ = 5.2 Hz, 1H), 5.77 (m, 2H), 6.48 (m, 2H), 7.18 (m, 5H), 7.79 (d, $J$ = 8.4 Hz, 1H). $^{13}$C NMR ($CDCl_3$, 100 MHz) $\delta$ 24.9, 25.4, 25.5, 25.7, 28.3, 33.2,35.5, 35.7, 45.1, 45.2, 54.8, 55.6, 55.6, 62.6, 69.2, 69.5, 70.6, 72.3, 73.1, 100.1, 104.3, 109.2, 115.0, 117.6, 118.0, 126.3, 128.3, 129.2, 134.0, 134.5, 137.5, 137.9, 155.0, 157.6, 164.9. FTIR (NaCl) $\nu_{max}$ = 1323, 1595, 1722, 2922, 3487 cm$^{-1}$. ESI (+) HRMS (*m/z*): $[M + H]^+$ calcd for $C_{37}H_{52}N_2O_9S$ 701.3472; found, 701.3473.

**Inhibitors 20a and 21a.** Compound **19a** (100 mg, 0.14 mmol) was dissolved in $CH_2Cl_2$ (90 mL). Grubbs' second-generation catalyst (12 mg, 0.014 mmol) was added, and the reaction was allowed to stir overnight at 23 °C. Solvent was removed under reduced pressure and the material purified by silica gel column chromatography (50:50 → 75:25 EtOAc:hexanes) to give 92 mg (96% yield) of product as a mixture of stereoisomers (31:69 *Z*/*E* by HPLC) as a white solid. The individual stereoisomers were isolated by reversed-phase HPLC YMC-Pack ODSA (250 mm × 10 mm, 5 $\mu$m); flow rate = 1.5 mL/min; isocratic 80:20 MeOH:$H_2O$; $T$ = 25 °C; $\lambda$ = 210 nm, $R_t$ *Z* = 17 min, $R_t$ *E* = 18 min).

**Compound 21a.** $[\alpha]_D^{20}$ −0.8 (*c* 2.36, $CHCl_3$). $^1$H NMR ($CDCl_3$, 800 MHz) $\delta$ 1.05 (s, 3H), 1.12 (s, 3H), 1.24 (t, $J$ = 6.4 Hz, 1H), 1.25 (s, 1H), 1.39 (m, 1H), 1.58 (m, 1H), 1.90−1.72 (m, 4H), 1.94−2.10 (m, 4H), 2.68 (dd, $J$ = 9.6, 14.4 Hz, 1H), 2.86 (q, $J$ = 7.2 Hz, 1H), 2.92 (dd, $J$ = 4, 14.4 Hz, 1H), 2.97 (dd, $J$ = 2.4, 15.2 Hz, 1H), 3.11 (dd, $J$ = 9.6, 15.2 Hz, 1H), 3.64 (m, 1H), 3.68 (m, 1H), 3.71 (dd, $J$ = 6.4, 13.6 Hz, 1H), 3.77 (m, 1H), 3.82 (m, 1H), 3.84 (s, 3H), 4.04−3.88 (m, 4H), 4.71 (d, $J$ = 9.6 Hz, 1H), 4.98 (q, $J$ = 7.2 Hz, 1H), 5.60 (d, $J$ = 5.6 Hz, 1H), 5.62 (d, $J$ = 5.6 Hz, 1H), 5.68 (m, 1H), 6.47 (m, 1H), 6.50 (dd, $J$ = 1.6, 8.8 Hz, 1H), 7.12 (d, $J$ = 7.2 Hz, 2H), 7.18 (t, $J$ = 7.2 Hz, 1H), 7.24 (t, $J$ = 8 Hz, 2H), 7.79 (d, $J$ = 8.8 Hz, 1H). $^{13}$C NMR ($CDCl_3$, 125 MHz) $\delta$ 25.7, 26.1, 27.6, 29.2, 29.6, 29.7, 35.6, 35.8, 45.3, 46.1, 54.7, 55.7, 56.1, 63.0, 69.6, 69.7, 70.7, 72.2, 73.3, 100.6, 104.4, 109.3, 117.8, 126.5, 128.4, 128.5, 129.3, 133.6, 134.5, 137.5, 155.1, 158.1, 164.9. FTIR (film, NaCl) $\nu_{max}$ = 3445, 2926, 1720, 1596, 1575, 1469, 1369 cm$^{-1}$. ESI (+) HRMS (*m/z*): $[M + Na]^+$ calcd for $C_{35}H_{48}N_2O_9S$ 695.2978; found, 695.2989.

**Compound 20a.** $[\alpha]_D^{20}$ −0.5 (*c* 0.99, $CHCl_3$). $^1$H NMR ($CDCl_3$, 800 MHz) $\delta$ 1.07 (s, 3H), 1.13 (s, 3H), 1.25 (s, 3H), 1.38 (m, 1H), 1.57 (m, 1H), 1.62−1.76 (m, 2H), 1.90 (br s, 2H), 1.98−2.20 (m, 4H), 2.70 (dd, $J$ = 9.6, 14.4 Hz, 1H), 2.86 (m, 1H), 2.91 (dd, $J$ = 0.8, 15.2 Hz, 1H), 2.93 (dd, $J$ = 4, 14.4 Hz, 1H), 3.08 (dd, $J$ = 8.8, 15.2 Hz, 1H), 3.65 (m, 1H), 3.68 (dd, $J$ = 6.4, 9.6 Hz, 1H), 3.79 (m, 1H), 3.82 (dt, $J$ = 2.4, 8.8 Hz, 1H), 3.85 (s, 3H), 3.93 (dd, $J$ = 6.4, 9.6 Hz, 1H), 3.96 (m, 1H), 4.08 (t, $J$ = 4.8 Hz, 2H), 4.74 (d, $J$ = 9.6 Hz, 1H), 4.98 (q, $J$ = 5.6 Hz, 1H), 5.53 (q, $J$ = 8.8 Hz, 1H), 5.62 (d, $J$ = 5.6 Hz, 1H), 5.65 (q, $J$ = 8.8 Hz, 1H), 6.47 (d, $J$ = 2.4 Hz, 1H), 6.51 (dd, $J$ = 2.4, 8.8 Hz, 1H), 7.13 (d, $J$ = 7.2 Hz, 2H), 7.18 (d, $J$ = 7.2 Hz, 1H), 7.23 (t, $J$ = 8 Hz, 2H), 7.81 (d, $J$ = 8.8 Hz, 1H). $^{13}$C NMR ($CDCl_3$, 125 MHz) $\delta$ 164.9, 157.9, 155.1, 137.5, 134.8, 131.0, 129.3, 128.4, 126.7, 126.5, 117.3, 109.3, 104.1, 100.2, 73.3, 72.6, 70.7, 69.6, 68.8, 64.1, 56.1, 55.7, 54.7, 45.3, 40.5, 36.1, 35.6, 29.7, 27.4, 26.7, 26.1, 25.8, 25.3. FTIR (film, NaCl) $\nu_{max}$ = 3344, 2925, 1718, 1595, 1575, 1388 cm$^{-1}$. $[M + Na]^+$ calcd for $C_{35}H_{48}N_2O_9S$ 695.2978; found, 695.2970.

**Compound 22a.** The corresponding olefin **20a** or **21a** (22 mg, 0.032 mmol) was dissolved in ethyl acetate (5 mL). Pd/C (10%) was added and the reaction flask flushed with $H_2$ gas. After stirring overnight, the reaction was filtered over celite and purified by silica chromatography (50:50 → 75:25 EtOAc:hexanes) to give 19 mg (90% yield) of the desired product. $[\alpha]_D^{20}$ −2.9 (*c* 0.70, $CHCl_3$). $^1$H NMR ($CDCl_3$, 800 MHz) $\delta$ 0.97 (s, 3H), 1.03 (s, 3H), 1.18 (m, 1H), 1.27 (m, 2H), 1.38 (m, 3H), 1.45 (m, 4H), 1.54−1.64 (m, 3H), 1.69 (m, 1H), 1.81 (m, 2H), 2.71 (dd, $J$ = 9.6, 14.4 Hz, 1H), 2.87 (m, 1H), 2.98 (dd, $J$ = 4, 14.4 Hz, 1H), 3.01 (dd, $J$ = 1.6, 15.2 Hz, 1H), 3.19 (dd, $J$ = 9.6, 15.2 Hz, 1H), 3.63−3.70 (m, 2H), 3.80 (m, 1H), 3.82 (dt, $J$ = 1.6, 8 Hz, 1H), 3.86 (s, 3H), 3.93 (dd, $J$ = 6.4, 9.6 Hz, 1H), 3.94 (m, 1H), 4.07 (m, 1H), 4.10 (m, 1H), 4.75 (d, $J$ = 9.6 Hz, 1H), 4.98 (q, $J$ = 5.6 Hz, 1H), 5.63 (d, $J$ = 4.8 Hz, 1H), 6.51 (m, 2H), 7.15 (d, $J$ = 7.2 Hz, 2H), 7.18 (t, $J$ = 7.2 Hz, 1H), 7.24 (t, $J$ = 8 Hz, 2H), 7.82 (d, $J$ = 8.8 Hz, 1H). $^{13}$C NMR ($CDCl_3$, 125 MHz) $\delta$ 19.6, 22.3, 25.0, 25.4, 25.8, 26.2, 27.4, 28.3, 35.7, 35.8, 39.8, 45.3, 54.8, 55.7, 56.1, 61.8, 68.9, 69.6, 70.7, 72.5, 73.3, 100.2, 104.0, 109.3, 117.7, 126.5, 128.4, 129.3, 135.6, 137.5, 155.1, 158.1, 164.9. FTIR (NaCl) $\nu_{max}$ = 3449, 2930, 1718, 1596, 1534 cm$^{-1}$. ESI (+) HRMS (*m/z*): $[M+H]^+$ calcd for $C_{35}H_{50}N_2O_9S$ 675.3315; found, 675.3318.

***tert*-Butyl-(2*S*,3*R*)-3-hydroxy-4-(2-methylpent-4-enylamino)-1-phenylbutan-2-ylcarbamate (17b and 17c).** A mixture of 2-methylpent-4-en-1-amine (460 mg, 4.6 mmol) and epoxide **8** (361.5 mg, 1.3 mmol) was allowed to stir at 60 °C overnight under argon atmosphere. The crude material was purified by silica gel column chromatography (3:97 MeOH:$CH_2Cl_2$) to give **17b** and **17c** (470 mg, 95%) as a white solid as a mix of diastereomers (50:50 by NMR); mp 89−90 °C; $[\alpha]_D^{20}$ +5.4 (*c* 2.58, $CHCl_3$). $^1$H NMR ($CDCl_3$, 400 MHz) $\delta$ 0.91 (d, $J$ = 2 Hz, 3H), 0.92 (d, $J$ = 2.4 Hz, 3H), 1.35 (s, 18H), 1.67 (m, 2H), 1.92 (m, 2H), 2.13 (m, 2H), 2.40 (dd, $J$ = 6.8, 11.6 Hz, 2H), 2.52 (dd, $J$ = 6, 12 Hz, 2H), 2.60−3.01 (m, 10H), 3.45 (m, 2H), 3.59−3.45 (m, 4H), 4.55−4.77 (m, 2H), 5.04 (m, 4H), 5.77 (m, 2H), 7.22 (m, 6H), 7.29 (m, 4H). $^{13}$C NMR ($CDCl_3$, 100 MHz) $\delta$ 17.8, 28.3, 33.2, 36.7, 39.2, 39.2, 51.4, 51.4, 54.1, 55.7, 70.6, 79.3, 116.0, 126.3, 128.4, 129.5, 137.0, 137.9, 155.9. FTIR (NaCl) $\nu_{max}$ = 3365, 1683, 1520, 1455, 1391, cm$^{-1}$. ESI (+) LRMS *m/z* (relative intensity): 363.03 $[M + H]^+$.

Pure **17c** was prepared in a similar fashion by using enantiopure (*S*)-2-methylpent-4-en-1-amine. $^1$H NMR ($CDCl_3$, 400 MHz) $\delta$ 0.99 (d, $J$ = 6 Hz, 3H, 1.32 (s, 9H), 1.99 (m, 2H), 2.12 (m, 1H), 2.70−2.95 (m, 4H), 3.08 (m, 2H), 3.80 (m, 2H), 5.04 (s, 1H), 5.07 (m, 1H), 5.71 (m, 1H), 6.41 (br s, 3H), 7.15−7.34 (m, 5H).

***tert*-Butyl-(2*S*,3*R*)-4-(2-(hex-5-enyloxy)-4-methoxy-*N*-(2-methylpent-4-enyl)phenylsulfonamido)-3-hydroxy-1-phenylbutan-2-ylcarbamate (18b and 18c).** A mixture of amines **17b** and **17c** (166 mg, 0.46 mmol) and sulfonyl chloride **7d** (167 mg, 0.55 mmol) were cooled to 0 °C. Pyridine (5 mL) was added and the solution stirred overnight. Solvents were removed by reduced pressure and the crude material purified by silica gel column chromatography (20:80 EtOAc:hexanes) to give a mixture of **18b** and **18c** (148 mg, 51% yield) as a colorless oil. $[\alpha]_D^{20}$ −1.8 (*c* 0.67, $CHCl_3$). $^1$H NMR ($CDCl_3$, 300 MHz) $\delta$ 0.80 (d, $J$ = 6 Hz, 3H), 0.88 (d, $J$ = 6 Hz, 3H), 1.33 (s, 18H), 1.52−1.65 (m, 4H), 1.70−1.92 (m, 9H), 2.06−2.26 (m, 6H), 3.36−2.80 (m, 12H), 3.73 (br, 4H), 3.84 (s, 6H), 4.06−3.94 (m, 5H), 4.59 (m, 2H), 4.90−5.06 (m, 8H), 5.58−5.87 (m, 4H), 6.44−6.54 (m, 4H), 7.16−7.30 (m, 10H), 7.83 (d, $J$ = 8.7 Hz, 2H). $^{13}$C NMR ($CDCl_3$, 75 MHz) $\delta$ 17.1, 25.0, 28.2, 28.3, 31.7, 31.9, 33.2, 35.3, 38.7, 53.2, 53.3, 54.4, 54.6, 55.6, 56.8, 57.1, 69.1, 2.3, 72.7, 79.4, 100.2, 104.1, 115.1, 116.3, 119.0,

126.3, 128.3, 129.5, 133.7, 136.3, 137.7, 137.9, 138.1, 155.9, 157.6, 164.7. FTIR (NaCl) $\nu_{max}$ = 3392, 2929, 1702, 1640, 1445, 1391, 1366, $cm^{-1}$. ESI (+) HRMS (*m/z*): $[M + H]^+$ calcd for $C_{34}H_{50}N_2O_7S$ 631.3417; found, 631.3408.

Pure **18c** was prepared in a similar fashion using pure **17c**. $^1H$ NMR ($CDCl_3$, 400 MHz) $\delta$ 0.80 (d, $J$ = 6 Hz, 3H), 1.34 (s, 9H), 1.59 (m, 2H), 1.74 (m, 2H), 1.87 (m, 2H), 2.12 (q, $J$=7.2 Hz, 2H), 2.19 (m, 1H), 2.94 (m, 3H), 3.25 (m, 3H), 3.74 (m, 2H), 3.85 (s, 3H), 3.96 (m, 1H), 4.03 (t, $J$=6.8 Hz, 2H), 4.57 (d, $J$=7.2 Hz, 1H), 4.93−5.05 (m, 4H), 5.66 (m, 1H), 5.80 (m, 1H), 6.46 (d, $J$= 2.4 Hz, 1H), 6.50 (dd, $J$ = 2.4, 8.8 Hz, 1H), 7.20 (m, 3H), 7.27 (m, 2H), 7.84 (d, $J$ = 8.4 Hz, 1H). $^{13}C$ NMR ($CDCl_3$, 100 MHz) $\delta$ 17.1, 25.0, 28.2, 28.4, 31.8, 33.3, 35.2, 38.1, 53.2, 54.5, 55.7, 56.9, 9.1, 72.3, 79.5, 100.2, 104.1, 115.1, 116.3, 119.1, 126.3, 128.4, 129.6, 133.7, 136.4, 137.7, 138.1, 155.9, 157.6, 164.7.

**(3*R*,3a*S*,6a*R*)-Hexahydrofuro[2,3-*b*]furan-3-yl (2*S*,3*R*)-4-(2-(hex-5-enyloxy)-4-methoxy-*N*-(2-methylpent-4-enyl)phenylsulfonamido)-3-hydroxy-1-phenylbutan-2-ylcarbamate (19b and 19c).** To a stirred solution of **18b** and **18c** (140 mg, 0.22 mmol) in $CH_2Cl_2$ (4.5 mL) was added TFA (1.5 mL). The resulting mixture was stirred for 4 h and then quenched with saturated aqueous $NaHCO_3$ (1.5 mL). Then 2N NaOH was added until the solution turned basic. The aqueous layer was extracted with ether, washed with brine, and dried over $Na_2SO_4$. Solvents were removed under reduced pressure to give crude *N*-((2*R*,3*S*)-3-amino-2-hydroxy-4-phenylbutyl)-2-(hex-5-enyloxy)-4-methoxy-*N*-(2-methylpent-4-enyl)benzensulfonamide.

To the above crude amine in MeCN (5 mL) were added (3*R*,3a*S*,6a*R*)-hexahydrofuro[2,3-*b*]furan-3-yl 4-nitrophenyl carbonate **12** (71 mg, 0.24 mmoL) and *i*-$Pr_2NEt$ (0.75 mL) under argon atmosphere and the reaction stirred overnight. Solvents were removed under reduced pressure and the crude material purified by silica gel column chromatography (50:50 EtOAc:hexanes) to give 68 mg (45% yield) of product as a clear oil. $[\alpha]_D^{20}$ −5.7 (*c* 0.17, $CHCl_3$). $^1H$ NMR ($CDCl_3$, 400 MHz) $\delta$ 0.80 (d, $J$ = 6.4 Hz, 3H) 0.90 (d, $J$ = 6.4 Hz, 3H), 1.40−2.24 (m, 22H), 2.70−3.40 (m, 14H), 3.62−4.06 (m, 24H), 4.92−5.05 (m, 12H), 5.60−5.85 (m, 6H), 6.50 (m, 4H), 7.18 (m, 6H), 7.24 (m, 4H), 7.83 (d, $J$ = 8.8 Hz, 2H). $^{13}C$ NMR ($CDCl_3$, 100 MHz) $\delta$ 17.1, 25.0, 25.7, 28.4, 31.9, 32.1, 33.2, 35.4, 38.1, 38.7, 45.3, 53.2, 53.4, 54.9, 55.0, 55.7, 56.9, 57.3, 69.2, 69.6, 70.7, 72.3, 72.8, 73.3, 100.3, 104.2, 109.2, 115.1, 116.5, 118.7, 118.8, 126.5, 128.4, 129.3, 133.8, 136.2, 137.5, 137.6, 138.0, 155.3, 157.6, 164.8. FTIR (film, NaCl) $\nu_{max}$ = 3436, 2970, 2927, 1718, 1600, 1458, 1374 $cm^{-1}$. ESI (+) HRMS (*m/z*): $[M + Na]^+$ calcd for $C_{36}H_{50}N_2O_9S$ 709.3135; found, 709.3131.

Pure **19c** was prepared in a similar fashion using pure **18c**. $^1H$ NMR ($CDCl_3$, 400 MHz) $\delta$ 0.81 (d, $J$=6 Hz, 3H), 1.45−1.90 (m, 8H), 2.12 (m, 2H), 2.23 (m, 1H), 2.80 (dd, $J$=9.2, 14 Hz, 1H), 2.93 (m, 3H), 3.15 (dd, $J$ = 2.4, 15.2 Hz, 1H), 3.24 (dd, $J$=8, 14 Hz, 1H), 3.38 (dd, $J$ = 9.2, 15.6 Hz, 1H), 3.65−3.75 (m, 3H), 3.77−3.89 (m, 6H), 3.95 (dd, $J$ = 6.4, 9.6 Hz, 1H), 4.05 (t, $J$=6.8 Hz, 2H), 4.85−5.05 (m, 6H), 5.62−5.85 (m, 3H), 6.48 (d, $J$=2.4 Hz, 1H), 6.52 (dd, $J$ = 2, 8.8 Hz, 1H), 7.20 (m, 3H), 7.26 (m, 2H), 7.84 (d, $J$ = 8.8 Hz, 1H). ESI (+) HRMS (*m/z*): $[M + Na]^+$ calcd for $C_{36}H_{50}N_2O_9S$ 709.3135; found, 709.3139.

**Inhibitors 20b, 20c, 21b, and 21c.** To a solution of carbamates **19b** and **19c** (119 mg, 0.17 mmol) in $CH_2Cl_2$ (125 mL) was added Grubb's second-generation catalyst (15 mg, 0.02 mmol). The resulting solution was stirred overnight. The solvent was removed under reduced pressure and the crude material purified by silica gel chromatography (50:50 EtOAc: hexanes) to give 110 mg (97% yield) of product as an oil. Reversed-phase HPLC (Waters Sunfire $C_{18}$ 50 mm × 4.6 mm, 5 $\mu$m coupled to Agilent Eclipse XDB $C_{18}$ 150 mm × 4.6 mm, 5 $\mu$m and YMC-Pack $C_8$ 250 mm × 4.6 mm, 5 $\mu$m, flow rate = 0.95 mL/min, $\lambda$ = 215 nm, $T$ = 30 °C, isocratic 60:40 MeCN:$H_2O$) was used to isolate the individual isomers: $R_t$ (*RZ*) = 22 min, $R_t$ (*SZ*) = 24 min, $R_t$ (*RE*) = 25.3 min, $R_t$ (*SE*) = 26.8 min.

**Compound 20b.** $[\alpha]_D^{20}$ −29 (*c* 0.60, $CHCl_3$). $^1H$ NMR ($CDCl_3$, 800 MHz) $\delta$ 1.12 (d, $J$ = 6.4 Hz, 3H) 1.50−1.62(m, 2H), 1.73 (m, 2H), 1.86 (m, 1H), 1.95 (m, 1H), 2.01−2.11 (m, 3H), 2.18 (m, 1H), 2.74 (dd, $J$ = 9.6, 14.4 Hz, 1H), 2.81 (d, $J$ = 15.2 Hz, 1H), 2.87 (m, 1H), 2.99 (dt, $J$=4, 13.6 Hz, 2H), 3.16 (dd, $J$ = 9.6, 15.2 Hz, 1H), 3.65−3.75 (m, 5H), 3.79−3.85 (m, 2H), 3.85 (s, 3H), 3.93 (dd, $J$ = 6.4, 9.6 Hz, 1H), 4.11 (m, 2H), 4.25 (m, 1H), 4.84 (d, $J$ = 9.6 Hz, 1H), 4.99 (q, $J$ = 6.4 Hz, 1H), 5.44 (q, $J$=9.6 Hz, 1H), 5.57 (q, $J$=7.2 Hz, 1H), 5.63 (d, $J$ = 4.8 Hz, 1H), 6.48 (d, $J$ = 1.6 Hz, 1H), 6.50 (dd, $J$ = 2.4, 8.8 Hz, 1H), 7.17 (m, 3H), 7.24 (m, 2H), 7.86 (d, $J$=8.8 Hz, 1H). $^{13}C$ NMR ($CDCl_3$, 125 MHz) $\delta$ 17.4, 25.4, 25.8, 26.1, 27.5, 32.2, 32.8, 35.7, 45.3, 53.9, 54.7, 55.7, 59.1, 68.4, 69.6, 70.7, 73.0, 73.3, 100.3, 103.9, 109.3, 118.1, 126.5, 127.2, 128.4, 129.4, 131.1, 134.4, 137.5, 155.2, 157.8, 164.9. FTIR (film, NaCl) $\nu_{max}$ = 3467, 2923, 1717, 1595, 1444, 1384, 1256 $cm^{-1}$. ESI (+) HRMS (*m/z*): $[M + Na]^+$ calcd for $C_{34}H_{46}N_2O_9S$ 681.2822; found, 681.2829.

**Compound 20c.** $[\alpha]_D^{20}$ −30.6 (*c* 0.83, $CHCl_3$). $^1H$ NMR ($CDCl_3$, 800 MHz) $\delta$ 1.13 (d, $J$ = 7.2 Hz, 3H) 1.61 (m, 1H), 1.69 (m, 1H), 1.78−1.90 (m, 4H), 1.94−2.09 (m, 5H), 2.18 (m, 1H), 2.74 (dd, $J$=8.8, 13.6 Hz, 1H), 2.89 (m, 2H), 2.96 (dd, $J$= 3.2, 13.6 Hz, 1H), 3.11 (dd, $J$=8, 14.4 Hz, 1H), 3.65−3.74 (m, 3H), 3.78−3.86 (m, 6H), 3.88−4.02 (m, 4H), 4.84 (d, $J$=8.8 Hz, 1H), 5.00 (q, $J$ = 5.6 Hz, 1H), 5.52 (m, 1H), 5.64 (d, $J$ = 4.8 Hz, 1H), 5.66 (m, 1H), 6.78 (d, $J$ = 2.4 Hz, 1H), 6.50 (dd, $J$=1.6, 8.8 Hz, 1H), 7.17 (m, 3H), 7.25 (m, 2H), 7.83 (d, $J$ = 8.8 Hz, 1H). $^{13}C$ NMR ($CDCl_3$, 125 MHz) $\delta$ 18.4, 25.8, 26.2, 28.6, 29.7, 30.0, 32.3, 35.4, 37.9, 45.3, 54.4, 54.8, 55.7, 58.1, 58.5, 69.6, 70.8, 72.6, 73.4, 100.7, 104.3, 109.3, 118.8, 126.5, 128.1, 128.5, 129.3, 133.3, 134.0, 137.6, 155.3, 158.1, 164.8. FTIR (NaCl) $\nu_{max}$ = 3442, 3339, 2924, 1717, 1595, 1495, 1444, 1325, 1256, 1206 $cm^{-1}$. ESI (+) HRMS (*m/z*): $[M + Na]^+$ calcd for $C_{34}H_{46}N_2O_9S$ 681.2822; found, 681.2825.

**Compound 21b.** $[\alpha]_D^{20}$ +27.6 (*c* 0.36, $CHCl_3$). $^1H$ NMR ($CDCl_3$, 800 MHz) $\delta$ 1.09 (d, $J$ = 6.4 Hz, 3H) 1.50−1.60 (m, 2H), 1.72 (m, 1H), 1.86 (m, 2H), 1.94−2.12 (m, 4H), 2.18 (m, 1H), 2.78 (dd, $J$ = 10.4, 14.4 Hz, 1H), 2.90 (m, 2H), 3.02 (dd, $J$=4.8, 14.4 Hz, 1H), 3.12 (dd, $J$ = 4, 14.4 Hz, 1H), 3.17 (m, 2H), 3.46 (m, 1H), 3.64−3.71 (m, 3H), 3.84−3.90 (m, 5H), 3.96 (m, 2H), 4.12 (m, 1H), 4.15 (m, 1H), 4.88 (d, $J$ = 8.8 Hz, 1H), 5.00 (q, $J$ = 8 Hz, 1H), 5.47 (q, $J$ = 8.8 Hz, 1H), 5.57 (q, $J$=7.2 Hz, 1H), 5.64 (d, $J$=5.6 Hz, 1H), 6.49 (m, 2H), 7.20 (m, 3H), 7.27 (m, 2H), 7.83 (d, $J$ = 8.8 Hz, 1H). $^{13}C$ NMR ($CDCl_3$, 125 MHz) $\delta$ 18.0, 25.3, 25.8, 26.0, 27.3, 32.2, 32.7, 35.4, 45.3, 53.3, 55.1, 55.7, 58.0, 68.4, 69.6, 70.9, 72.3, 73.4, 100.2, 104.0, 109.3, 118.3, 126.5, 127.6, 128.5, 129.3, 130.8, 134.3, 137.7, 155.6, 157.8, 164.8. FTIR (film, NaCl) $\nu_{max}$ = 3467, 2927, 1717, 1595, 1456, 1325, $cm^{-1}$. ESI (+) HRMS (*m/z*): $[M + Na]^+$ calcd for $C_{34}H_{46}N_2O_9S$ 681.2822; found, 681.2819.

**Compound 21c.** $[\alpha]_D^{20}$ +20.5 (*c* 1.17, $CHCl_3$). $^1H$ NMR ($CDCl_3$, 800 MHz) $\delta$ 1.06 (d, $J$ = 6.4 Hz, 3H), 1.47 (m, 1H), 1.63 (m, 1H), 1.70−1.82 (m, 4H), 1.87 (m, 1H), 1.93 (m, 1H), 2.17 (m, 2H), 2.26 (m, 1H), 2.47 (br, 1H), 2.76 (dd, $J$ = 8.8, 14.4 Hz, 1H), 2.91 (m, 2H), 2.98 (m, 2H), 3.55 (m, 1H), 3.69 (m, 2H), 3.75 (m, 1H), 3.80 (m, 1H), 3.85 (m, 4H), 3.88 (t, $J$ = 8.8 Hz, 1H), 3.94 (dd, $J$ = 6.4, 9.6 Hz, 1H), 4.11 (m, 1H), 4.17 (br, 1H), 4.76 (d, $J$ = 9.6 Hz, 1H), 5.00 (q, $J$ = 8 Hz, 1H), 5.53 (m, 1H), 5.64 (d, $J$ = 4.8 Hz, 1H), 5.67 (m, 1H), 6.47 (d, $J$ = 2.4 Hz, 1H), 6.50 (dd, $J$=2.4, 8.8 Hz, 1H), 7.14 (d, $J$=7.2 Hz, 2H), 7.18 (m, 1H), 7.24 (t, $J$ = 7.2 Hz, 2H),7.83 (d, $J$ = 8.8 Hz, 1H). $^{13}C$ NMR ($CDCl_3$, 125 MHz) $\delta$ 19.0, 25.8, 26.2, 28.1, 29.8, 30.3, 33.6, 35.7, 38.2, 45.3, 54.6, 54.9, 55.7, 58.6, 69.6, 70.8, 71.5, 73.4, 100.5, 104.2, 109.3, 119.0, 126.5, 128.5, 129.4, 129.6, 132.5, 134.2, 137.4, 155.2, 158.1, 164.8. FTIR (film, NaCl) $\nu_{max}$ = 3463, 3339, 1717, 1595, 1495, 1387, 1326 $cm^{-1}$. ESI(+) HRMS (*m/z*): $[M + Na]^+$ calcd for $C_{34}H_{46}N_2O_9S$ 681.2822; found, 681.2812.

**Compound 22b.** To a stirred solution of the corresponding (*R*)-*E* olefin (8 mg, 0.013 mmol) was dissolved into EtOAc (5 mL) a spatula tip of Pd on carbon (10 wt %) and the mixture was stirred under $H_2$ atmosphere. The reaction stirred overnight.

Solvents were removed under reduced pressure, and the crude material was purified by silica gel column chromatograph (70:30 $Et_2O$:hexanes → 100% $Et_2O$) to give **22b** (8 mg, quantitative yield) as a white solid. TLC 100% $Et_2O$. $[\alpha]_D^{23}$ −7.8 (*c* 0.84, $CHCl_3$). $^1H$ NMR ($CDCl_3$, 500 MHz) $\delta$ 0.92 (d, $J$ = 7 Hz, 3H) 1.16−1.84 (m, 15H), 2.74 (dd, $J$ = 9.5, 14 Hz, 1H), 2.89 (m, 1H), 3.05 (m, 3H), 3.28 (m, 2H), 3.65−3.87 (m, 9H), 3.94 (m, 1H), 4.10 (m, 1H), 4.21 (m, 1H), 4.84 (d, $J$ = 9.5 Hz, 1H), 5.01 (q, $J$ = 7 Hz, 1H), 5.64 (d, $J$ = 5.5 Hz, 1H), 6.51 (m, 2H), 7.19 (m, 3H), 7.26 (m, 2H), 7.88 (d, $J$ = 9.5 Hz, 1H). $^{13}C$ NMR ($CDCl_3$, 125 MHz) $\delta$ 17.8, 23.4, 23.5, 25.5, 25.8, 26.1, 27.5, 31.8, 31.9, 35.7, 45.3, 52.5, 54.8, 55.2, 55., 68.8, 69.6, 70.7, 71.3, 73.3, 100.4, 104.0, 109.3, 118.0, 126.5, 128.5, 129.4, 134.4, 137.6, 155.2, 158.0, 165.0. FTIR (NaCl) $\nu_{max}$ = 3463, 2924, 2853, 1721, 1596, 1323, 1256 $cm^{-1}$. ESI(+) HRMS (*m/z*): $[M + Na]^+$ calcd for $C_{34}H_{48}N_2O_9S$ 683.2978; found, 683.2987.

**Compound 22c.** To a solution of the corresponding (*S*)-*E* olefin (12 mg, 0.018 mmol) in EtOAc (5 mL) a spatula tip of Pd on carbon (10 wt %) was added and the mixture was stirred under $H_2$ atmosphere. The reaction was stirred overnight. Solvents were removed under reduced pressure and the crude material purified by silica chromatograph (70:30 $Et_2O$:hexanes → 100% $Et_2O$) to give **22c** (9 mg, 78% yield) as a white solid. $[\alpha]_D^{23}$ −6.6 (*c* 0.91, $CHCl_3$). $^1H$ NMR ($CDCl_3$, 800 MHz) $\delta$ 0.90 (d, $J$ = 6.4 Hz, 3H) 1.20−1.90 (m, 15H), 2.73 (m, 1H), 2.79 (dd, $J$ = 8.8, 13.6 Hz, 1H), 2.90 (m, 1H), 2.96 (m, 1H), 3.08 (m 1H), 3.33 (dd, $J$ = 9.6, 15.2 Hz, 1H), 3.47 (m, 1H), 3.61 (m, 1H), 3.70 (m, 2H), 3.85 (m, 6H), 3.95 (m, 1H), 4.10 (m, 1H), 4.25 (m, 1H), 4.86 (d, $J$ = 8.8 Hz, 1H), 5.03 (q, $J$ = 7.2 Hz, 1H), 5.65 (d, $J$ = 4.8 Hz, 1H), 6.52 (m, 2H), 7.18 (m, 3H), 7.25 (m, 2H), 7.87 (d, $J$ = 9.6 Hz, 1H). $^{13}C$ NMR ($CDCl_3$, 200 MHz) $\delta$ 18.4, 23.4, 24.3, 25.0, 25.8, 26.5, 27.2, 32.8, 33.1, 35.4, 45.3, 53.5, 54.8, 55.7, 57.0, 69.3, 69.6, 70.8, 72.2, 73.3, 100.6, 104.2, 109.3, 118.0, 126.5, 128.5, 129.4, 134.5, 137.5, 155.3, 158.1, 165.1. FTIR (NaCl) $\nu_{max}$ = 3463, 2854, 1717, 1596, 1444, 1323, 1256 $cm^{-1}$. ESI (+) HRMS (*m/z*): $[M + Na]^+$ calcd for $C_{34}H_{48}N_2O_9S$ 683.2978; found, 683.2976.

**Determination of X-ray Structures of HIV-1 Protease (wt)−Inhibitor Complexes for Inhibitors 14c and 2. X-ray Structure for 14c.** The HIV-1 protease construct with the substitutions Q7K, L33I, L63I, C67A, and C95A to optimize protein stability without altering protease structure and activity was expressed and purified as described.[23,24] Crystals were grown by the hanging drop vapor diffusion method using 1:15 molar ratio of protease at 2.0 mg/mL and inhibitor **14c** dissolved in dimethylsulfoxide. The reservoir contained 5% glycerol, 0.5 M NaI in 0.2 M MES buffer with pH 6.0. Subsequently, crystals were mounted on nylon loops in liquid nitrogen with additional 28% glycerol (v/v) as cryoprotectant. X-ray diffraction data were collected on SER-CAT 22-ID beamline of the Advanced Photon Source, Argonne National Laboratory, with wavelength 0.8 Å under the stream of liquid nitrogen at 90 K. Data were processed by HKL2000,[25] resulting in $R_{merge}$ of 10.8% for **14c**, and the structure was solved by molecular replacement with our previous structure (PDB code 3B7V) using PHASER[26] in CCP4i Suite,[27,28] refined by SHELX-97,[29,30] and refitted manually with the graphic programs O10,[31] and COOT.[32] The inhibitor structure was modeled by PRODRG-2,[33] which also provided restraints for refinement. The crystal structure of HIV-1 protease with inhibitor **14c** was determined at 1.17 Å resolution. The rmsd for Cα atoms in comparison with our wild type protease with DRV (PDB code 2IEN[19]) is only 0.33 Å . Alternate conformations were modeled for the protease residues when obvious in the electron density maps. Anisotropic atomic displacement parameters (*B* factors) were applied for all atoms including solvent molecules. The occupancies of iodine atoms were refined and varied from 0.24 to 0.60. Hydrogen atoms were added at the final stages of the refinement. The final structure includes 2 $Na^+$ ions, 19 $I^-$ ions, 2 glycerols, and 181 waters in PR-**14c** complex. The *R* factor and $R_{free}$ are 16.0 and 19.4%. The crystallographic statistics are listed in Table 1 (Supporting Information). The crystal structure and structure factors have been deposited in the RCSB Protein Data Bank,[34] with PDB code 3I6O for inhibitor **14c**.

**X-ray Structure for 2.** The wild-type HIV-1 protease was expressed and purified as described previously.[35] After purification, the protease was concentrated to 4.0 mg/mL. Inhibitor **2**, at a 10-fold molar excess, was mixed with the protease. The mixture was incubated at room temperature for 2 h and then clarified with a 0.2 mm spin filter. The crystallization trials employed the hanging drop method using equal volumes of enzyme−inhibitor and well solution. The reservoir contained 20% $(NH4)_2SO_4$, 200 mM $NaPO_4$/citric acid buffer, pH 5.5. The well solutions also included 10% dimethyl sulfoxide, 30 mM β-mercaptoethanol, and 4% isopropyl alcohol.

Diffraction data were collected at room temperature with an Raxis-IV image plate and integrated and reduced with the HKL program package.[25] The diffraction data set has a resolution of 1.7 Å with an $R_{merge}$ value of 0.052. Data completeness was 95.5%. The space group was determined to be $P2_12_12_1$ with unit cell dimensions of $a$ = 51.9 Å, $b$ = 59.0 Å, $c$ = 62.6 Å, with one dimer in the asymmetric unit. The initial phase was solved by molecular replacement using the program AMoRe.[36] A protease dimer (PDB code 2AID)[37] from a previously determined HIV-1 protease crystal structure was used as the search model. Crystallographic refinement was carried out using X-PLOR 3.1. Molecular graphics program O[31] was used for map display and model building. Water molecules were added to the structure as identified in the $|F_o| - |F_c|$ map contoured at the 3σ level. Data collection and refinement statistics are listed in Table 2 (Supporting Information). The final $R_{work}$ was 21.6% and $R_{free}$ was 28.9% for data between the resolution of 20 and 1.7 Å (Table 1). The rmsd values from ideal bond distances and angles were 0.009 Å and 1.5°, respectively. The average *B* factor was 28.3 and 19.6 $Å^2$ for protein and inhibitor atoms, respectively, and 41.0 $Å^2$ for solvent atoms. The crystal structures and structure factors have been deposited in the RCSB Protein Data Bank,[34] with PDB code 3I7E for inhibitor **2**.

**Acknowledgment.** The research was supported by grants from the National Institutes of Health (GM53386, A.K.G., and GM062920, I.T.W.). This work was also supported by the Intramural Research Program of the Center for Cancer Research, National Cancer Institute, National Institutes of Health, and in part by a Grant-in-Aid for Scientific Research (Priority Areas) from the Ministry of Education, Culture, Sports, Science, and Technology of Japan (Monbu Kagakusho), a Grant for Promotion of AIDS Research from the Ministry of Health, Welfare, and Labor of Japan (Kosei Rohdosho: H15-AIDS-001), and the Grant to the Cooperative Research Project on Clinical and Epidemiological Studies of Emerging and Reemerging Infectious Diseases (Renkei Jigyo: no. 78, Kumamoto University) of Monbu-Kagakusho. We thank the staff at the SER-CAT beamline at the Advanced Photon Source, Argonne National Laboratory, for assistance during X-ray data collection. Use of the Advanced Photon Source was supported by the U.S. Department of Energy, Office of Science, Office of Basic Energy Sciences, under contract no. DE-AC02-06CH11357. We thank Dr. John Harwood, Purdue University, for many helpful discussions surrounding NMR spectroscopy.

**Supporting Information Available:** HPLC and HRMS data of all inhibitors; crystallographic data collection and refinement statistics. This material is available free of charge via the Internet at http://pubs.acs.org.

## References

(1) *2007 AIDS Epidemic Update*; UNAIDS, WHO, December, 2007.

(2) Spekowitz, K. A. AIDS—The First 20 Years. *Engl. J. Med.* **2001**, *344*, 1764–1772.
(3) Hertogs, K.; Bloor, S.; Kemp, S. D.; Van den Enyde, C.; Alcorn, T. M.; Pauwels, R.; Van Houtte, M.; Staszewski, S.; Miller, V.; Larder, B. A Phenotypic and genotypic analysis of clinical HIV-1 isolated reveals extensive protease inhibitor cross-resistance: a survey of over 6000 samples. *AIDS* **2000**, *14*, 1203–1210.
(4) (a) Ghosh, A. K.; Kincaid, J. F.; Cho, W.; Walters, D. E.; Krishnan, K.; Hussain, K. A.; Koo, Y.; Cho, H.; Holland, J.; Buthod, J. Potent HIV-1 inhibitors incorporating high-affinity P2-ligands and (*R*)-(hydroxyethylamino)sulofonamide isostere. *Bioorg. Med. Chem. Lett.* **1998**, *8*, 687–690. (b) Koh, Y.; Nakata, H.; Maeda, K.; Ogata, H.; Bilcer, G.; Devasamudram, T.; Kincaid, J. F.; Boross, P.; Wang, Y.-F.; Tie, Y.; Volarath, P.; Gaddis, L.; Harrison, R. W.; Weber, I. T.; Ghosh, A. K.; Mitsuya, H. A novel bis-tetrahydrofuranylurethane-containing non-peptide protease inhibitor (PI) UIC-94017 (TMC-114) potent against multi-PI-resistant HIV in vitro. *Antimicrob. Agents Chemother.* **2003**, *47*, 3123–3129. (c) Ghosh, A. K.; Pretzer, E.; Cho, H.; Hussain, K. A.; Duzgunes, N. Antiviral activity of UIC-PI, a novel inhibitor of human immunodeficiency virus type 1 protease. *Antiviral Res.* **2002**, *54*, 29–36.
(5) Surleraux, D. L. N. G.; Tahri, A.; Verchueren, W. G.; Pille, G. M. E.; de Kock, H. A.; Jonckers, T. H. M.; Peeters, A.; De Meyer, S; Azijn, H.; Pauwels, R.; de Bethune, M. −P.; King, N. M.; Prabu-Jeyabalan, M.; Schiffer, C. A.; Wigerinck, P. B. T. P. Discovery and selection of TMC-114, a next generation of HIV-1 protease inhibitor. *J. Med. Chem.* **2005**, *48*, 1813–1822.
(6) (a) Yoshimura, K.; Kato, R.; Kavlick, M. F.; Nguyen, A.; Maroun, V.; Maeda, K.; Husssin, K. A.; Ghosh, A. K.; Gulnik, S. V.; Erickson, J. W.; Mitsuya, H. A. A potent human immunodeficiency virus type 1 protease inhibitor, UIC-94003 (TMC-126), and selection of a novel (A28S) mutation in the protease active site. *J. Virol.* **2002**, *76*, 1349–1358. (b) Koh, Y.; Nakata, H.; Maeda, K.; Ogata, H.; Bilcer, G.; Devasamudram, T.; Kincaid, J. F.; Boross, P.; Wang, Y.-F.; Tie, Y.; Volarath, P.; Gaddis, L.; Harrison, R. W.; Weber, I. T.; Ghosh, A. K.; Mitsuya, H. A novel bis-tetrahydrofuranylurethane-containing non-peptide protease inhibitor (PI) UIC-94017 (TMC-114) potent against multi-PI-resistant HIV in vitro. *Antimicrob. Agents Chemother.* **2003**, *47*, 3123–3129.
(7) Ghosh, A. K.; Chapsal, B. D.; Weber, I. T.; Mitsuya, H. Design of HIV protease inhibitors targeting protein backbone: an effective strategy for combating drug resistance. *Acc. Chem. Res.* **2008**, *41*, 78–86.
(8) On June 23, 2006, FDA approved new HIV treatment for patients who do not respond to existing drugs. Please see: http://www.fda.gov/bbs/topics/NEWS/2006/NEW01395.html.
(9) On October 21, 2008, FDA granted traditional approval to Prezista (darunavir), coadministered with ritonavir and with other antiretroviral agents, for the treatment of HIV-1 infection in treatment-experienced adult patients. In addition to the traditional approval, a new dosing regimen for treatment-naïve patients was approved.
(10) Tie, Y.; Boross, P. I.; Wang, Y. F.; Gaddis, L.; Hussain, A. K.; Leshchenko, S.; Ghosh, A. K.; Louis, J. M.; Harrison, R. W.; Weber, I. T. High resolution crystal structures of HIV-1 protease with a potent non-peptide inhibitor (UIC-94017) active against multidrug-resistant clinical strains. *J. Mol. Biol.* **2004**, *338*, 341–352.
(11) Kovalevsky, A. Y.; Tie, Y.; Liu, F.; Boross, P. I.; Wang, Y. F.; Leshchenko, S.; Ghosh, A. K.; Harrison, R. W.; Weber, I. T. Effectiveness of nonpeptide clinical inhibitor TMC-114 on HIV-1 protease with highly drug resistant mutations D30N, I50 V, and L90M. *J. Med. Chem.* **2006**, *49*, 1379–1387.
(12) Kempf, D. J.; Marsh, K. C.; Paul, D. A.; Knige, M. F.; Norbeck, D. W.; Kohlbrenner, W. E.; Codacovi, L.; Vasavanonda, S.; Bryant, P.; Wang, X. C.; Wideburg, N. E.; Clement, J. J.; Plattner, J. J.; Erickson, J. Antiviral and Pharmacokinetic Properties of C2-Symmetric Inhibitors of the Human Immunodeficiency Virus Type 1 Protease. *Antimicrob. Agents Chemother.* **1991**, *35*, 2209–2214.
(13) Baldwin, E. T.; Bhat, T. N.; Liu, B.; Pattabriaman, N.; Erickson, J. W. Structural Basis of Drug Resistance for V82A mutant of HIV-1 Proteinase. *Nat. Struct. Biol.* **1995**, *2*, 244–49.
(14) Mitsunobu, O. The use of diethyl azodicarboxylate and triphenylphosphine in synthesis and transformation of natural products. *Synthesis* **1981**, 1–28.
(15) Ghosh, A. K.; Sridhar, P. R.; Kumaragurubaran, N.; Koh, Y.; Weber, I. T.; Mitsuya, H. Bis-Tetrahydrofuran: a Privileged Ligand for Darunavir and a New Generation of HIV Protease Inhibitors That Combat Drug Resistance. *ChemMedChem* **2006**, *1*, 937–950.
(16) (a) Schwab, P.; France, M. B.; Ziller, J. W.; Grubbs, R. H. A Series of Well-Defined Metathesis Catalysts—Synthesis of $[RuCl_2(=CHR')(PR_3)_2]$ and Its Reactions. *Angew. Chem., Int. Ed. Engl.* **1995**, *34*, 2039–2041. (b) Scholl, M.; Ding, S.; Lee, C.; Grubbs, R. H. Synthesis and Activity of a New Generation of Ruthenium-Based Olefin Metathesis Catalysts Coordinated with 1,3-Dimesityl-4,5-dihydroimidazol-2-ylidene Ligands. *Org. Lett.* **1999**, *1*, 953–956.
(17) Toth, M. V.; Marshall, G. R. A simple, continuous fluorometric assay for HIV protease. *Int. J. Pept. Protein Res.* **1990**, *36*, 544–550.
(18) Gustchina, A.; Sansom, C.; Prevost, M.; Richelle, J.; Wodak, S.; Wlodawer, A.; Weber, I. Energy calculations and analysis of HIV-1 protease-inhibitor crystal structures. *Protein Eng.* **1994**, *7*, 309–317.
(19) Tie, Y.; Boross, P. I.; Wang, Y. F.; Gaddis, L.; Liu, F.; Chen, X.; Tozser, J.; Harrison, R. W.; Weber, I. T. Molecular basis for substrate recognition and drug resistance from 1.1 to 1.6 Å resolution crystal structures of HIV-1 protease mutants with substrate analogs. *FEBS J.* **2005**, *272*, 5265–5277.
(20) Panigrahi, S.; Desiraju, G. Strong and weak hydrogen bonds in the protein−ligand interface. *Proteins* **2007**, *67*, 128–141.
(21) Steiner, T. Hydrogen bonds from water molecules to aromatic acceptors in very high-resolution protein crystal structures. *Biophys. Chem.* **2002**, *95*, 195–201.
(22) Wang, Y. F.; Tie, Y.; Boross, P. I.; Tozser, J.; Ghosh, A. K.; Harrison, R. W.; Weber, I. T. Potent new antiviral compound shows similar inhibition and structural interactions with drug resistant mutants and wild type HIV-1 protease. *J. Med. Chem.* **2007**, *50*, 4509–4515.
(23) Louis, J. M.; Clore, G. M.; Gronenborn, A. M. Autoprocessing of HIV-1 protease is tightly coupled to protein folding. *Nat. Struct. Biol.* **1999**, *6*, 868–875.
(24) Mahalingam, B.; Louis, J. M.; Hung, J.; Harrison, R. W.; Weber, I. T. Structural implications of drug resistant mutants of HIV-1 protease: high resolution crystal structures of the mutant protease/substrate analog complexes. *Proteins* **2001**, *43*, 455–464.
(25) Otwinowski, Z.; Minor, W. Processing of X-ray Diffraction Data Collected in Oscillation Mode. *Methods in Enzymology, 276: Macromolecular Crystallography, Part A*; Carter, C.W., Jr., Sweet, R. M., Eds.; Academic Press: New York, 1997; pp 307−326.
(26) McCoy, A. J.; Grosse-Kunstleve, R. W.; Adams, P. D.; Winn, M. D.; Storoni, L. C.; Read, R. J. Phaser crystallographic software. *J. Appl. Crystallogr.* **2007**, *40*, 658–674.
(27) Collaborative Computational Project, Number 4 The CCP4 Suite: Programs for Protein Crystallography. *Acta Crystallogr., Sect. D: Biol. Crystallogr.*, **1994**, *50*, 760−763.
(28) Potterton, E.; Briggs, P.; Turkenburg, M.; Dodson, E. A graphical user interface to the CCP4 program suite. *Acta Crystallogr., Sect. D: Biol. Crystallogr.* **2003**, *59*, 1131–1137.
(29) Sheldrick, G. M. A short history of SHELX. *Acta Crystallogr., Sect. A: Found. Crystallogr.* **2008**, *64*, 112–122.
(30) Sheldrick, G. M.; Schneider, T. R. SHELXL: high resolution refinement. *Methods Enzymol.* **1997**, *277*, 319–343.
(31) Jones, T. A.; Zou, J. Y.; Cowan, S. W.; Kjeldgaard, M. Improved methods for building protein models in electron density maps and the location of errors in these models. *Acta Crystallogr., Sect. A: Found. Crystallogr.* **1991**, *47*, 110–119.
(32) Emsley, P.; Cowtan, K. Coot: Model-Building Tools for Molecular Graphics. *Acta Crystallogr., Sect. D: Biol. Crystallogr.* **2004**, *60*, 2126–2132.
(33) Schuettelkopf, A. W.; van Aalten, D. M. F. PRODRG—a tool for high-throughput crystallography of protein−ligand complexes.". *Acta Crystallogr., Sect. D: Biol. Crystallogr.* **2004**, *60*, 1355–1363.
(34) Berman, H. M.; Westbrook, J.; Feng, Z.; Gilliland, G.; Bhat, T. N.; Weissig, H.; Shindyalov, I. N.; Bourne, P. E. The Protein Data Bank. *Nucleic Acids Res.* **2000**, *28*, 235–242.
(35) Hong, L.; Treharne, A.; Hartsuck, J. A.; Foundling, S.; Tang, J. Crystal Structures of Complexes of a Peptidic Inhibitor with Wild-Type and Two Mutant HIV-1 Protease. *Biochemistry* **1996**, *35*, 10627–10633.
(36) Navaja, J. A. MoRe: An Automated Package for Molecular Replacement. *Acta Crystallogr., Sect. A: Found. Crystallogr.* **1994**, *50*, 157–163.
(37) Rutenber, E.; Fauman, E. B.; Keenan, R. J.; Fong, S.; Furth, P. S.; Ortiz de Montellano, P. R.; Meng, E.; Kuntz, I. D.; DeCamp, D. L.; Salto, R. Structure of a non-peptide inhibitor complexed with HIV-1 protease. Developing a cycle of structure-based drug design. *J. Biol. Chem.* **1993**, *268*, 15343–15346.

ANTIMICROBIAL AGENTS AND CHEMOTHERAPY, Sept. 2009, p. 3887–3893 Vol. 53, No. 9
0066-4804/09/$08.00+0 doi:10.1128/AAC.00270-09


# Potent Activity of a Nucleoside Reverse Transcriptase Inhibitor, 4′-Ethynyl-2-Fluoro-2′-Deoxyadenosine, against Human Immunodeficiency Virus Type 1 Infection in a Model Using Human Peripheral Blood Mononuclear Cell-Transplanted NOD/SCID Janus Kinase 3 Knockout Mice▽

Shinichiro Hattori,[1] Kazuhiko Ide,[2] Hirotomo Nakata,[4] Hideki Harada,[1] Shinya Suzu,[1] Noriyuki Ashida,[3] Satoru Kohgo,[3] Hiroyuki Hayakawa,[3] Hiroaki Mitsuya,[2,4] and Seiji Okada[1]*

*Division of Hematopoiesis, Center for AIDS Research,[1] and Department of Infectious Diseases and Department of Hematology,[2] Kumamoto University Graduate School of Medical and Pharmaceutical Sciences, Kumamoto, Japan; Biochemicals Division, Yamasa Corporation, Chiba, Japan[3]; and Experimental Retrovirology Section, HIV and AIDS Malignancy Branch, National Cancer Institute, National Institutes of Health, Bethesda, Maryland[4]*

Received 26 February 2009/Returned for modification 9 April 2009/Accepted 16 June 2009

**4′-Ethynyl-2-fluoro-2′-deoxyadenosine (EFdA), a recently discovered nucleoside reverse transcriptase inhibitor, exhibits activity against a wide spectrum of wild-type and multidrug-resistant clinical human immunodeficiency virus type 1 (HIV-1) isolates (50% effective concentration, 0.0001 to 0.001 μM). In the present study, we used human peripheral blood mononuclear cell-transplanted, HIV-1-infected NOD/SCID/Janus kinase 3 knockout mice for in vivo evaluation of the anti-HIV activity of EFdA. Administration of EFdA decreased the replication and cytopathic effects of HIV-1 without identifiable adverse effects. In phosphate-buffered saline (PBS)-treated mice, the $CD4^+/CD8^+$ cell ratio in the spleen was low (median, 0.04; range, 0.02 to 0.49), while that in mice receiving EFdA was increased (median, 0.65; range, 0.57 to 1.43). EFdA treatment significantly suppressed the amount of HIV-1 RNA (median of $9.0 \times 10^2$ copies/ml [range, $8.1 \times 10^2$ to $1.1 \times 10^3$ copies/ml] versus median of $9.9 \times 10^4$ copies/ml [range, $8.1 \times 10^2$ to $1.1 \times 10^3$ copies/ml]; $P < 0.001$), the p24 level in plasma ($2.5 \times 10^3$ pg/ml [range, $8.2 \times 10^2$ to $5.6 \times 10^3$ pg/ml] versus $2.8 \times 10^2$ pg/ml [range, $8.2 \times 10^1$ to $6.3 \times 10^2$ pg/ml]; $P < 0.001$), and the percentage of p24-expressing cells in the spleen (median of 1.90% [range, 0.33% to 3.68%] versus median of 0.11% [range, 0.00% to 1.00%]; $P = 0.003$) in comparison with PBS-treated mice. These data suggest that EFdA is a promising candidate for a new age of HIV-1 chemotherapy and should be developed further as a potential therapy for individuals with multidrug-resistant HIV-1 variants.**

Highly active antiretroviral therapy, combining two or more reverse transcriptase inhibitors and/or proteinase inhibitors, has been successful in reducing the morbidity and mortality caused by human immunodeficiency virus type 1 (HIV-1) infection (6, 27). The limitations of antiviral therapy for AIDS are exacerbated by the development of drug-resistant HIV-1 variants, the existence of viral reservoirs (4, 5), and a number of inherent adverse effects (1, 31). Nucleoside reverse transcriptase inhibitors (NRTIs), including zidovudine, didanosine, lamivudine, and stavudine, constitute the most important class of antiretroviral compounds for the treatment of HIV-1 infection (9, 17). However, the application of these compounds is clinically limited due to their cytotoxicity through inhibition of the host DNA polymerase and the rapid emergence of drug-resistant viral strains (2, 16). Therefore, developing new compounds with reduced cytotoxicity and improved antiviral potency, especially against drug-resistant viral strains, has become an urgent therapeutic objective. Recently, a new antiviral agent, 4′-ethynyl-2-fluoro-2′-deoxyadenosine (EFdA), was created (Fig. 1) (21, 23, 24). EFdA shows potent antiviral activity (50% effective concentration = 0.004 μM) and good activity against NRTI-resistant strains (10). Interestingly, EFdA-triphosphate (the active form of EFdA) showed more intracellular stability (21) and generated a more persistent antiviral effect than those of other NRTIs. In addition, EFdA is effective against human polymerases α, β, and γ, suggesting that EFdA might serve as a suitable therapy for treating individuals with HIV-1 infection and AIDS (21).

Severely immunodeficient mice transplanted with human peripheral blood mononuclear cells (hu-PBMC-SCID mice) represent a useful model for AIDS research, including preclinical evaluation of antiretroviral agents and vaccine development. Although the initial SCID mouse model required many PBMC for engraftment and showed inconsistent efficacy (20), recently introduced NK cell-deficient mice show a markedly improved engraftment efficiency. For this study, we established human PBMC-transplanted, $HIV\text{-}1_{JR\text{-}FL}$-infected nonobese diabetic (NOD)/SCID/Janus kinase 3 (Jak3) knockout (NOJ) mice, in which massive and systemic HIV-1 infection occurs, human $CD4^+/CD8^+$ cell ratios significantly decrease, and high

* Corresponding author. Mailing address: Division of Hematopoiesis, Center for AIDS Research, Kumamoto University, 2-2-1 Honjo, Kumamoto 860-0811, Japan. Phone: 81-96-373-6522. Fax: 81-96-373-6523. E-mail: okadas@kumamoto-u.ac.jp.

▽ Published ahead of print on 22 June 2009.

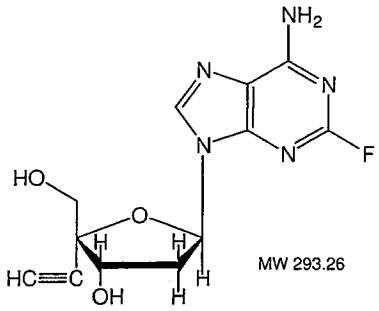


FIG. 1. Structure of EFdA.

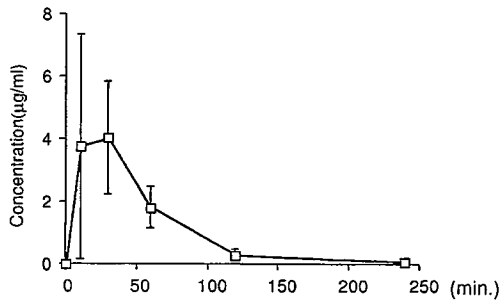


FIG. 2. Pharmacokinetics of EFdA. Each mouse was administered EFdA intraperitoneally at a dose of 20 mg/kg, and blood samples were taken at 15, 30, 60, 120, and 240 min ($n$ = 4).

levels of HIV-1 viremia are achieved. In these mice, the novel anti-HIV-1 agent EFdA, an NRTI, exerted potent anti-HIV-1 activity. Thus, our refined hu-PBMC-SCID mouse model is a powerful tool to evaluate antiretroviral activity and the adverse effects of new anti-HIV-1 agents.

## MATERIALS AND METHODS

**Antiviral agent.** EFdA was synthesized as published elsewhere (21, 23, 24).

**Pharmacokinetic analysis of EFdA in BALB/c mice.** Pharmacokinetic analysis of EFdA in BALB/c mice was performed as previously described (22). In brief, plasma samples were collected periodically for 4 h following a single EFdA administration at a dose of 20 mg/kg of body weight dissolved in 250 μl phosphate-buffered saline (PBS). Each plasma sample (50 μl) was centrifuged at 10,000 rpm for 10 min, and the supernatant was injected into a high-performance liquid chromatography system. The eluent was monitored by UV spectroscopy at 262 nm, and the EFdA concentration in plasma was determined.

To examine the adverse effects of high-dose EFdA treatment, EFdA was administered to BALB/c mice twice a day intraperitoneally at a dose of 5 to 50 mg/kg for 14 days, and we observed their status and body weight twice a week.

**Transplantation of human PBMC into NOJ mice.** NOJ mice were established and maintained in the Center for Animal Resources and Development, Kumamoto University (Kumamoto, Japan) (26). The mice were 16 to 20 weeks old at the time of transfer of human PBMC. Human PBMC-transplanted NOJ (hu-PBMC-NOJ) mice were generated by previously described methods (22). Briefly, NOJ mice were irradiated (1.8 Gy), and PBMC ($1 \times 10^7$) were freshly prepared from heparinized blood of a single healthy HIV-1-seronegative donor by Ficoll-Hypaque density gradient centrifugation, resuspended in PBS (0.1 ml), and infused intraperitoneally into each mouse. Peripheral blood was collected from healthy volunteers after informed consent was obtained, according to the institutional guidelines approved by the Faculty of Medical and Pharmaceutical Sciences, Kumamoto University. All animal experiments were performed according to the guidelines of the Kumamoto University Graduate School of Medical Science.

**Treatment of HIV-1-infected hu-PBMC-NOJ mice with EFdA.** Five days after PBMC implantation, HIV-$1_{JR\text{-}FL}$ (25,000 50% tissue culture infective doses) (12) was inoculated intraperitoneally into each mouse for which PBMC engraftment was confirmed. Twenty-four hours after HIV-1 inoculation, EFdA (10 μg in 0.1 ml PBS/mouse, twice a day) or PBS was administered for 14 consecutive days (see Fig. 3). On day 15, blood samples were collected from the mouse orbit, and then peritoneal cavity and spleen cells were harvested and resuspended in PBS.

**Flow cytometric analysis.** Reconstructed human PBMC proliferation in mice was determined by flow cytometric analysis with allophycocyanin (APC)-Cy7-conjugated anti-mouse CD45 (BD Pharmingen, San Diego, CA), Pacific Blue (PB)-conjugated anti-human CD45 (anti-hCD45), APC-conjugated anti-hCD4 (Dako Cytomation, Glostrup, Denmark), phycoerythrin (PE)-Cy7-conjugated anti-hCD3 (e-Bioscience, San Diego, CA), and fluorescein isothiocyanate (FITC)-conjugated anti-hCD8 (Beckman Coulter, Fullerton, CA) monoclonal antibodies. The cells were treated with red cell lysing buffer (155 mM $NH_4Cl$, 10 mM $KHCO_3$, and 0.1 mM EDTA) to lyse erythrocytes before staining. Single-cell suspensions were prepared in staining medium (PBS with 3% fetal bovine serum and 0.05% sodium azide) and stained with monoclonal antibodies as described above. After 30 min of incubation on ice, the cells were washed twice with washing medium, fixed in PBS with 0.1% paraformaldehyde for 20 min in the dark, and permeabilized in PBS with 0.01% saponin. After 10 min of incubation on ice, cells were stained with PE-conjugated anti-HIV-1 p24 monoclonal antibody (Beckman Coulter, Fullerton, CA) for 30 min on ice. After being stained, the cells were analyzed on an LSR II flow cytometer (BD Bioscience, San Jose, CA). Data were analyzed with FlowJo (Tree Star, San Carlos, CA) software.

**Quantification of murine plasma HIV-1 p24 and viral RNA copy numbers.** The amount of p24 antigen in murine plasma was determined using an HIV-1 p24 antigen enzyme-linked immunosorbent assay kit (ZeptoMetrix Corp., Buffalo, NY). The plasma viral load was quantified with the Amplicor HIV-1 Monitor test, version 1.5 (Roche Diagnostics, Branchburg, NJ).

**Statistical analysis.** Nonparametric statistical analyses were performed using the Mann-Whitney U test and StatView software, version 4.51.1 (Abacus Concepts, Berkeley, CA). $P$ values of $<0.05$ were defined as significant.

## RESULTS

**Pharmacokinetics of EFdA in BALB/c mice.** We examined the pharmacokinetics of EFdA in BALB/c mice by intraperitoneally administering the compound at a dose of 20 mg/kg. Plasma samples were collected periodically for up to 4 h and subjected to high-performance liquid chromatography analysis. As shown in Fig. 2, the concentration of EFdA reached the maximal concentration 10 to 30 min after intraperitoneal administration and then decreased rapidly. Although the initial blood concentration was highly variable, we found that the areas under the blood concentration-time curve were similar among the four mice (4.18, 2.44, 6.10, and 7.23 mg/liter-h; mean = 4.99 ± 1.68 mg/liter-h). Next, we administered EFdA intraperitoneally to BALB/c mice twice a day at a dose of 5 to 50 mg/kg for 14 days to examine the adverse effects induced by high-dose EFdA treatment. Mice treated with EFdA at doses of 5 to 50 mg/kg did not show any body weight loss (data not shown). No acute and subacute whole-body effects were observed in mice. Mice treated with 50 mg/kg showed ruffled fur, but the main organs of these mice appeared normal. These results suggest that even high doses of EFdA have few adverse effects in mice.

**Effects of EFdA on $CD4^+$ and $CD8^+$ cell counts in HIV-1-infected hu-PBMC-NOJ mice.** The in vivo antiviral potency of EFdA was investigated in the hu-PBMC-NOJ mouse model of HIV-1 infection. NOJ mice were intraperitoneally transplanted with human PBMC ($1 \times 10^7$ cells/mouse) 5 days before inoculation with HIV-$1_{JR\text{-}FL}$ (R5 strain). EFdA (10 μg/mouse; 0.5 mg/kg) was administered intraperitoneally twice a day for 15 days (Fig. 3). PBMC were recovered from murine peripheral blood, the peritoneal cavity, and the spleen on day 16 after HIV-1 inoculation. Samples were stained with anti-mouse CD45–APC-Cy7, anti-hCD45–PB, anti-CD3–PE-Cy7,

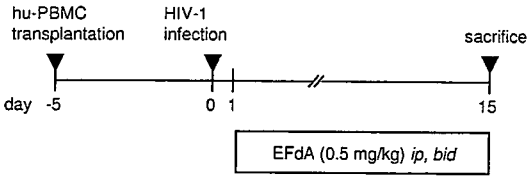


FIG. 3. Protocol for drug administration. ip, intraperitoneally; bid, twice daily.

anti-CD4–APC, and anti-CD8–FITC and subjected to flow cytometric analysis for the determination of $CD4^+/CD8^+$ cell ratios. As shown in Fig. 4A, distinct $CD4^+$ cells as well as $CD8^+$ cells were seen in PBMC recovered from uninfected PBMC-transplanted mice. There were only a few $CD4^+$ cells in PBMC recovered from HIV-$1_{JR\text{-}FL}$-infected, PBS-treated mice, resulting in a low CD4/CD8 ratio (median, 0.04; range, 0.02 to 0.49); however, the $CD4^+$ cell frequency was increased by EFdA treatment (median, 0.65; range, 0.57 to 1.43), up to the level in uninfected mice (median, 0.79; range, 0.73 to 1.43), in the PBMC as well as the spleen and peritoneal cavity (Fig. 4B). The numbers of $CD4^+$ cells in PBS-treated mouse peripheral blood, spleens, and peritoneal cavities were significantly lower than those in EFdA-treated ($P < 0.001$) or uninfected ($P < 0.005$) mice (Fig. 5), while there were no significant differences in $CD8^+$ cell numbers between groups, indicating that EFdA is not toxic to lymphocytes. Thus, EFdA protects $CD4^+$ T cells against HIV-1 infection-induced cell death.

**EFdA suppresses HIV-1 viremia in hu-PBMC-NOJ mice.** The amount of HIV-1 p24 in plasma was also found to be very high in PBS-treated mice (median, $1.9 \times 10^3$ pg/ml; range, $8.3 \times 10^2$ to $5.6 \times 10^3$ pg/ml). EFdA was found to significantly suppress the amount of plasma p24 on day 15 (median, $2.1 \times 10^2$ pg/ml; range, $8.3 \times 10^1$ to $6.3 \times 10^2$ pg/ml; $P < 0.001$) (Fig. 6A). We also determined the HIV-1 RNA copy number in infected, PBS-treated mice and found that the median copy number was $9.9 \times 10^4$ (range, $1.3 \times 10^4$ to $5.4 \times 10^5$) copies/ml on day 15 after HIV-1 inoculation; however, EFdA significantly suppressed viremia (median, $9.0 \times 10^2$ copies/ml; range, $8.1 \times 10^2$ to $1.1 \times 10^3$ pg/ml; $P < 0.001$) on day 15.

**Effects of EFdA on intracellular p24 levels in HIV-1-infected hu-PBMC-NOJ mice.** The number of p24-expressing ($p24^+$) cells in human $CD3^+$ cells in the spleen, peripheral blood, and peritoneal cavity was analyzed by flow cytometric analysis. The frequency of $p24^+$ cells in the spleen was found to be high for PBS-treated mice (median, 1.90%; range, 0.33% to 3.68%). EFdA was found to significantly suppress the level of $p24^+$ cells (median, 0.11%; range, 0.00% to 1.00%; $P = 0.003$) (Fig. 7A and B). The frequency of $p24^+$ cells in peripheral blood and the peritoneal cavity was also found to be high for PBS-



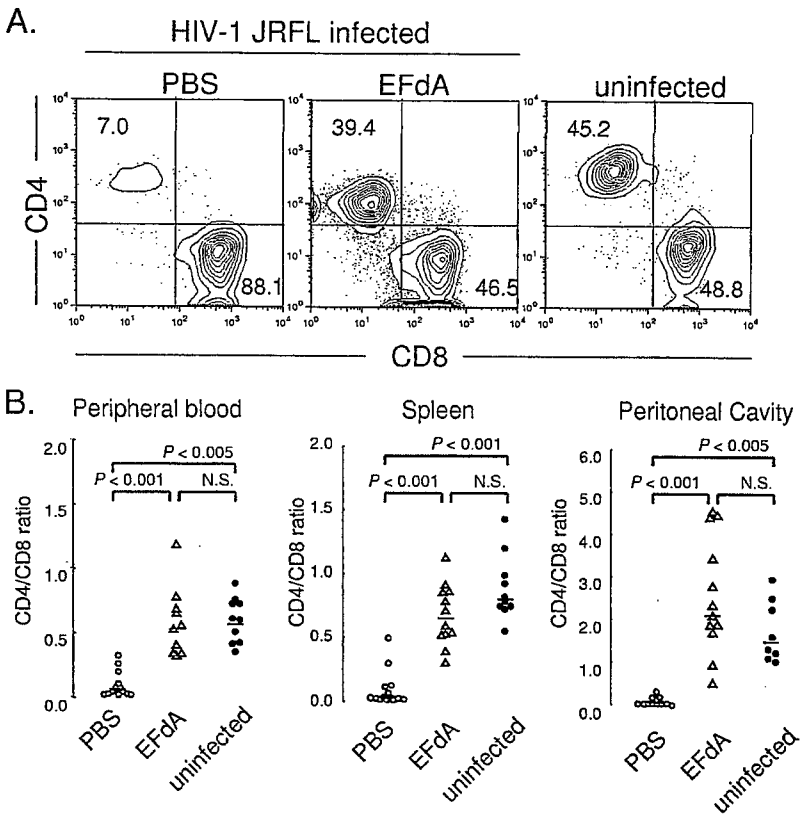


FIG. 4. Effects of EFdA on the $CD4^+/CD8^+$ cell ratio in HIV-1-infected hu-PBMC-NOJ mice. (A) PBMC recovered on day 16 after R5 HIV-$1_{JRFL}$ inoculation were subjected to flow cytometry. Representative flow cytometric analysis profiles are shown. (B) PBMC, spleen cells, and peritoneal cavity cells recovered on day 16 after HIV-1 inoculation were subjected to flow cytometry. CD4/CD8 ratios are shown for each mouse ($n = 12$).

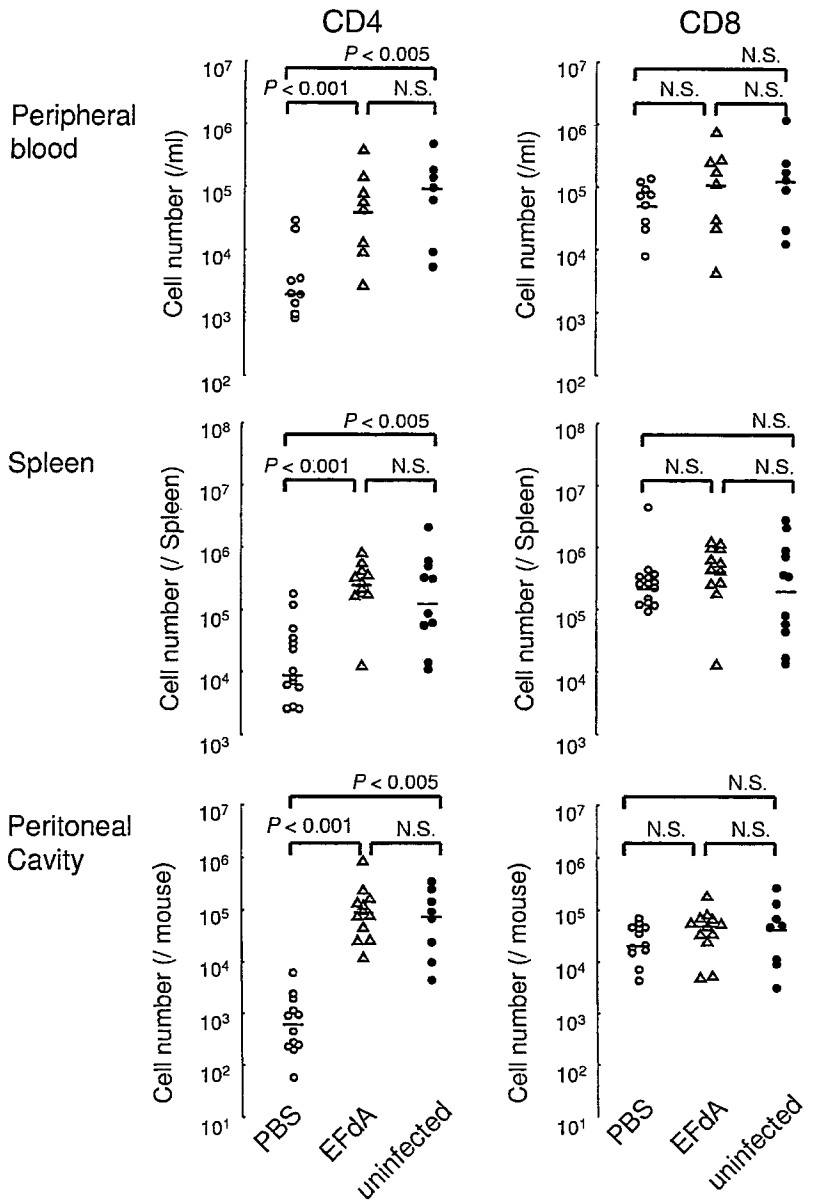


FIG. 5. Effects of EFdA on numbers of $CD4^+$ and $CD8^+$ cells. PBMC ($n$ = 9), spleen cells ($n$ = 12), and peritoneal cavity cells ($n$ = 12) recovered on day 16 after HIV-1 inoculation were counted and subjected to flow cytometry. Short bars indicate the medians. N.S., not significant.

treated mice and significantly suppressed after EFdA treatment. No apparent EFdA-associated adverse effects were seen throughout the study period.

## DISCUSSION

In the present study, we demonstrated the potent activity of EFdA as an agent against HIV in hu-PMBC-NOJ mice. As demonstrated, this particular model is well suited to the study of therapeutic interventions in the HIV arena, providing information on the treatment effects on $CD4^+$ T-cell counts as well as on viral markers, such as plasma p24, HIV-1 RNA, and intracellular p24, which are important parameters in determining the overall effectiveness of a treatment in HIV-1-positive patients.

SCID mice implanted with human PBMC, which are known as hu-PBMC-SCID mice, have been used as an animal model for investigating the pathogenesis of HIV infection (15, 18, 19); however, PBMC reconstitution of the SCID mouse varies considerably among transplantation methods, laboratories, experiments, graft sources, and even individual mice (20). PBMC transplantation into NOD/SCID animals resulted in a significant increase in the positive transplantation rate compared to that obtained by identical treatment of SCID animals (7, 13). More recently, the introduction of mice with a complete loss of NK cells, such as NOD/SCID/common $\gamma^{-/-}$ mice (8, 32),

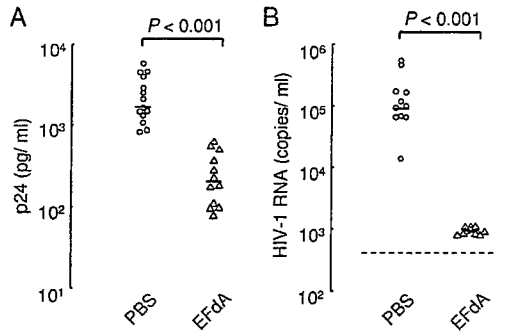


FIG. 6. Effects of EFdA on the amounts of plasma p24 and HIV-1 RNA. Blood samples were collected from the mouse orbit on day 16 after HIV-1 inoculation. (A) Amounts of plasma p24 antigen ($n$ = 12). (B) HIV-1 RNA copy numbers ($n$ = 11). Short bars indicate the medians.

BALB/c Rag-2$^{-/-}$ $\gamma^{-/-}$ mice (30), and NOJ mice (26), markedly improved the engraftment of PBMC as well as human hematopoietic stem cells and has enabled more stable and precise analysis (14, 22, 29). HIV-1 was challenged 2 weeks after peripheral blood lymphocyte (PBL) transplantation in the previous work (22, 28), since an HIV-1 R5 virus is not adequately infective soon after transplantation (3). We optimized the time of viral infection and found that $HIV_{JR-FL}$ could successfully infect cells and replicate during virus challenge as early as 5 days after PBL transplantation. Since the HIV-1-infected hu-PBL-NOJ mouse model needed a relatively smaller amount of human PBL and a shorter duration of HIV-1 infection and replication than those in previous studies (7, 13, 22, 28), it could be a more useful instrument for analyzing the pathogenesis of HIV-1 infection and testing the efficacy of antiviral agents.

A number of 4′-ethynyl (4′-E)-2′-deoxynucleosides and their analogs have been synthesized, and a series of potent anti-HIV-1 compounds have been identified to block the replication of a wide spectrum of laboratory and clinical HIV-1 strains in vitro (11, 23, 25). By optimization of such 4′-E nucleoside analogs, EFdA was found to have potent anti-HIV activity, including activity against highly multidrug-resistant variants, with favorable in vitro cell toxicities (21, 24). EFdA shows unique anti-HIV-1 function and characteristics. EFdA-triphosphate shows greater intracellular stability and generates a more persistent antiviral effect than those of other NRTIs, such as zidovudine or tenofovir. EFdA acts as a chain terminator upon incorporation at the primer end; however, it showed no inhibition of cellular polymerases (21). In addition,

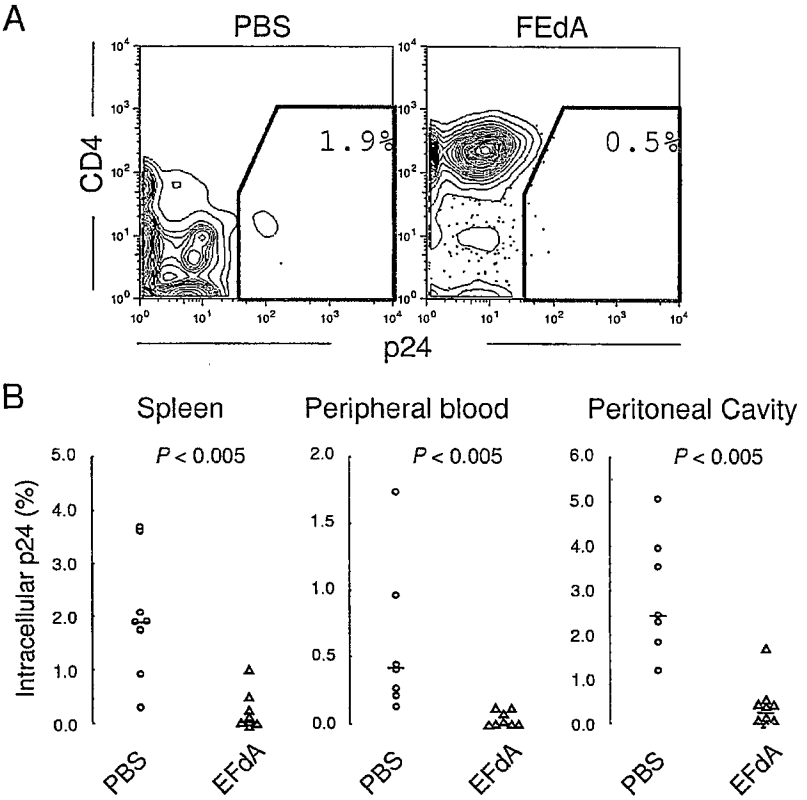


FIG. 7. Effects of EFdA on HIV-1-infected cells. (A) PBMC recovered on day 16 after $HIV\text{-}1_{JRFL}$ inoculation were stained with anti-p24–PE, anti-mouse CD45–APC-Cy7, anti-hCD45–PB, anti-hCD4–PB, anti-hCD4–APC, anti-hCD3–PE-Cy7, and anti-hCD8–FITC and subjected to flow cytometry. Representative flow cytometric analysis profiles of the mouse CD45$^-$ hCD45$^+$ hCD3$^+$ hCD8$^-$ gated fraction are shown. (B) PBMC, spleen cells, and peritoneal cavity cells recovered on day 16 after HIV-1 inoculation were subjected to flow cytometry. The percentage of p24$^+$ cells among CD4 T cells (CD45$^-$ hCD45$^+$ hCD3$^+$ hCD8$^-$ gated) is shown ($n$ = 8).

unlike other adenosine-based NRTIs, EFdA shows adenosine deaminase resistance (10), and moreover, it has a very high selectivity index, and high-dose EFdA is not toxic to BALB/c mice. In the present study, hu-PBMC-NOJ AIDS model mice treated with EFdA maintained high levels of human $CD4^+$ lymphocytes (Fig. 4 and 5), suppressed plasma levels of p24 and HIV-1 RNA (Fig. 6), and reduced the number of infected ($p24^+$) cells without apparent adverse effects. Although we cannot directly compare EFdA with previously studied anti-HIV-1 agents, our study suggests that EFdA is expected to be effective for clinical use and is a favorable anti-HIV-1 therapeutic agent. It is notable that determination of the precise pharmacokinetics and pharmacodynamics is awaited in clinical trials when EFdA is assessed in humans.

In summary, the data presented here provide strong evidence that the hu-PBMC-NOJ mouse is a valuable model for preclinical testing of new antiretroviral agents. Using this HIV-1 infection mouse model system, we have demonstrated that a new antiretroviral agent, EFdA, has potent anti-HIV-1 activity in vivo, without apparent adverse effects. Since EFdA has unique functional properties, low cytotoxicity, and superior persistence of antiviral activity, it is a promising candidate for a new age of HIV-1 chemotherapy.

## ACKNOWLEDGMENTS

We thank Yoshio Koyanagi (Institute for Virus Research, Kyoto University, Kyoto, Japan) for providing the $HIV\text{-}1_{JR\text{-}FL}$ strain, I. Suzu for technical assistance, and Y. Endo for secretarial assistance.

This work was supported in part by the intramural research program of the Center for Cancer Research, National Cancer Institute, National Institutes of Health, by science research grants from the Ministry of Health, Labor and Welfare of Japan, by a grant to the Cooperative Research Project on Clinical and Epidemiological Studies of Emerging and Reemerging Infectious Diseases (Renkei Jigyo, no. 78; Kumamoto University), and by grants from the Global COE program (Education Unit and Global Education and Research Center Aiming at the Control of AIDS) of the Ministry of Education, Culture, Sports, Science, and Technology of Japan.

## REFERENCES

1. **Carr, A., K. Samaras, A. Thorisdottir, G. R. Kaufmann, D. J. Chisholm, and D. A. Cooper.** 1999. Diagnosis, prediction, and natural course of HIV-1 protease-inhibitor-associated lipodystrophy, hyperlipidaemia, and diabetes mellitus: a cohort study. Lancet 353:2093–2099.
2. **Chen, C. H., and Y. C. Cheng.** 1989. Delayed cytotoxicity and selective loss of mitochondrial DNA in cells treated with the anti-human immunodeficiency virus compound 2',3'-dideoxycytidine. J. Biol. Chem. 264: 11934–11937.
3. **Fais, S., C. Lapenta, S. M. Santini, M. Spada, S. Parlato, M. Logozzi, P. Rizza, and F. Belardelli.** 1999. Human immunodeficiency virus type 1 strains R5 and X4 induce different pathogenic effects in hu-PBL-SCID mice, depending on the state of activation/differentiation of human target cells at the time of primary infection. J. Virol. 73:6453–6459.
4. **Finzi, D., J. Blankson, J. D. Siliciano, J. B. Margolick, K. Chadwick, T. Pierson, K. Smith, J. Lisziewicz, F. Lori, C. Flexner, T. C. Quinn, R. E. Chaisson, E. Rosenberg, B. Walker, S. Gange, J. Gallant, and R. F. Siliciano.** 1999. Latent infection of CD4+ T cells provides a mechanism for lifelong persistence of HIV-1, even in patients on effective combination therapy. Nat. Med. 5:512–517.
5. **Finzi, D., M. Hermankova, T. Pierson, L. M. Carruth, C. Buck, R. E. Chaisson, T. C. Quinn, K. Chadwick, J. Margolick, R. Brookmeyer, J. Gallant, M. Markowitz, D. D. Ho, D. D. Richman, and R. F. Siliciano.** 1997. Identification of a reservoir for HIV-1 in patients on highly active antiretroviral therapy. Science 278:1295–1300.
6. **Gulick, R. M., J. W. Mellors, D. Havlir, J. J. Eron, C. Gonzalez, D. McMahon, D. D. Richman, F. T. Valentine, L. Jonas, A. Meibohm, E. A. Emini, and J. A. Chodakewitz.** 1997. Treatment with indinavir, zidovudine, and lamivudine in adults with human immunodeficiency virus infection and prior antiretroviral therapy. N. Engl. J. Med. 337:734–739.
7. **Hesselton, R. M., D. L. Greiner, J. P. Mordes, T. V. Rajan, J. L. Sullivan, and L. D. Shultz.** 1995. High levels of human peripheral blood mononuclear cell engraftment and enhanced susceptibility to human immunodeficiency virus type 1 infection in NOD/LtSz-scid/scid mice. J. Infect. Dis. 172:974–982.
8. **Ishikawa, F., M. Yasukawa, B. Lyons, S. Yoshida, T. Miyamoto, G. Yoshimoto, T. Watanabe, K. Akashi, L. D. Shultz, and M. Harada.** 2005. Development of functional human blood and immune systems in NOD/SCID/IL2 receptor γ chain(null) mice. Blood 106:1565–1573.
9. **Jochmans, D.** 2008. Novel HIV-1 reverse transcriptase inhibitors. Virus Res. 134:171–185.
10. **Kawamoto, A., E. Kodama, S. G. Sarafianos, Y. Sakagami, S. Kohgo, K. Kitano, N. Ashida, Y. Iwai, H. Hayakawa, H. Nakata, H. Mitsuya, E. Arnold, and M. Matsuoka.** 2008. 2'-Deoxy-4'-C-ethynyl-2-halo-adenosines active against drug-resistant human immunodeficiency virus type 1 variants. Int. J. Biochem. Cell Biol. 40:2410–2420.
11. **Kodama, E. I., S. Kohgo, K. Kitano, H. Machida, H. Gatanaga, S. Shigeta, M. Matsuoka, H. Ohrui, and H. Mitsuya.** 2001. 4'-Ethynyl nucleoside analogs: potent inhibitors of multidrug-resistant human immunodeficiency virus variants in vitro. Antimicrob. Agents Chemother. 45:1539–1546.
12. **Koyanagi, Y., S. Miles, R. T. Mitsuyasu, J. E. Merrill, H. V. Vinters, and I. S. Chen.** 1987. Dual infection of the central nervous system by AIDS viruses with distinct cellular tropisms. Science 236:819–822.
13. **Koyanagi, Y., Y. Tanaka, J. Kira, M. Ito, K. Hioki, N. Misawa, Y. Kawano, K. Yamasaki, R. Tanaka, Y. Suzuki, Y. Ueyama, E. Terada, T. Tanaka, M. Miyasaka, T. Kobayashi, Y. Kumazawa, and N. Yamamoto.** 1997. Primary human immunodeficiency virus type 1 viremia and central nervous system invasion in a novel hu-PBL-immunodeficient mouse strain. J. Virol. 71:2417–2424.
14. **Macchiarini, F., M. G. Manz, A. K. Palucka, and L. D. Shultz.** 2005. Humanized mice: are we there yet? J. Exp. Med. 202:1307–1311.
15. **McCune, J., H. Kaneshima, J. Krowka, R. Namikawa, H. Outzen, B. Peault, L. Rabin, C. C. Shih, E. Yee, M. Lieberman, et al.** 1991. The SCID-hu mouse: a small animal model for HIV infection and pathogenesis. Annu. Rev. Immunol. 9:399–429.
16. **Medina, D. J., C. H. Tsai, G. D. Hsiung, and Y. C. Cheng.** 1994. Comparison of mitochondrial morphology, mitochondrial DNA content, and cell viability in cultured cells treated with three anti-human immunodeficiency virus dideoxynucleosides. Antimicrob. Agents Chemother. 38:1824–1828.
17. **Mitsuya, H., R. Yarchoan, and S. Broder.** 1990. Molecular targets for AIDS therapy. Science 249:1533–1544.
18. **Mosier, D. E.** 1991. Adoptive transfer of human lymphoid cells to severely immunodeficient mice: models for normal human immune function, autoimmunity, lymphomagenesis, and AIDS. Adv. Immunol. 50:303–325.
19. **Mosier, D. E., R. J. Gulizia, S. M. Baird, D. B. Wilson, D. H. Spector, and S. A. Spector.** 1991. Human immunodeficiency virus infection of human-PBL-SCID mice. Science 251:791–794.
20. **Murphy, W. J., D. D. Taub, and D. L. Longo.** 1996. The huPBL-SCID mouse as a means to examine human immune function in vivo. Semin. Immunol. 8:233–241.
21. **Nakata, H., M. Amano, Y. Koh, E. Kodama, G. Yang, C. M. Bailey, S. Kohgo, H. Hayakawa, M. Matsuoka, K. S. Anderson, Y. C. Cheng, and H. Mitsuya.** 2007. Activity against human immunodeficiency virus type 1, intracellular metabolism, and effects on human DNA polymerases of 4'-ethynyl-2-fluoro-2'-deoxyadenosine. Antimicrob. Agents Chemother. 51:2701–2708.
22. **Nakata, H., K. Maeda, T. Miyakawa, S. Shibayama, M. Matsuo, Y. Takaoka, M. Ito, Y. Koyanagi, and H. Mitsuya.** 2005. Potent anti-R5 human immunodeficiency virus type 1 effects of a CCR5 antagonist, AK602/ONO4128/GW873140, in a novel human peripheral blood mononuclear cell nonobese diabetic-SCID, interleukin-2 receptor γ-chain-knocked-out AIDS mouse model. J. Virol. 79:2087–2096.
23. **Ohrui, H.** 2006. 2'-Deoxy-4'-C-ethynyl-2-fluoroadenosine, a nucleoside reverse transcriptase inhibitor, is highly potent against all human immunodeficiency viruses type 1 and has low toxicity. Chem. Rec. 6:133–143.
24. **Ohrui, H., S. Kohgo, H. Hayakawa, E. Kodama, M. Matsuoka, T. Nakata, and H. Mitsuya.** 2007. 2'-Deoxy-4'-C-ethynyl-2-fluoroadenosine: a nucleoside reverse transcriptase inhibitor with highly potent activity against wide spectrum of HIV-1 strains, favorable toxic profiles, and stability in plasma. Nucleosides Nucleotides Nucleic Acids 26:1543–1546.
25. **Ohrui, H., and H. Mitsuya.** 2001. 4'-C-substituted-2'-deoxynucleosides: a family of antiretroviral agents which are potent against drug-resistant HIV variants. Curr. Drug Targets Infect. Disord. 1:1–10.
26. **Okada, S., H. Harada, T. Ito, T. Saito, and S. Suzu.** 2008. Early development of human hematopoietic and acquired immune systems in new born NOD/Scid/Jak3(null) mice intrahepatic engrafted with cord blood-derived CD34 (+) cells. Int. J. Hematol. 88:476–482.
27. **Palella, F. J., Jr., K. M. Delaney, A. C. Moorman, M. O. Loveless, J. Fuhrer, G. A. Satten, D. J. Aschman, S. D. Holmberg, et al.** 1998. Declining morbidity and mortality among patients with advanced human immunodeficiency virus infection. N. Engl. J. Med. 338:853–860.
28. **Ruxrungtham, K., E. Boone, H. Ford, Jr., J. S. Driscoll, R. T. Davey, Jr., and H. C. Lane.** 1996. Potent activity of 2'-beta-fluoro-2',3'-dideoxyadenosine against human immunodeficiency virus type 1 infection in hu-PBL-SCID mice. Antimicrob. Agents Chemother. 40:2369–2374.

29. **Shultz, L. D., F. Ishikawa, and D. L. Greiner.** 2007. Humanized mice in translational biomedical research. Nat. Rev. Immunol. **7**:118–130.
30. **Traggiai, E., L. Chicha, L. Mazzucchelli, L. Bronz, J. C. Piffaretti, A. Lanzavecchia, and M. G. Manz.** 2004. Development of a human adaptive immune system in cord blood cell-transplanted mice. Science **304**:104–107.
31. **Walker, U. A., B. Setzer, and N. Venhoff.** 2002. Increased long-term mitochondrial toxicity in combinations of nucleoside analogue reverse-transcriptase inhibitors. AIDS **16**:2165–2173.
32. **Yahata, T., K. Ando, Y. Nakamura, Y. Ueyama, K. Shimamura, N. Tamaoki, S. Kato, and T. Hotta.** 2002. Functional human T lymphocyte development from cord blood CD34+ cells in nonobese diabetic/Shi-scid, IL-2 receptor gamma null mice. J. Immunol. **169**:204–209.

# Prediction of Potency of Protease Inhibitors Using Free Energy Simulations with Polarizable Quantum Mechanics-Based Ligand Charges and a Hybrid Water Model

Debananda Das,[†] Yasuhiro Koh,[‡] Yasushi Tojo,[‡] Arun K. Ghosh,[§] and Hiroaki Mitsuya*[,†,‡]

Experimental Retrovirology Section, HIV and AIDS Malignancy Branch, National Cancer Institute, National Institutes of Health, Bethesda, Maryland 20892-1868, Departments of Hematology and Infectious Diseases, Kumamoto University Graduate School of Medical and Pharmaceutical Sciences, Kumamoto 860-8556, Japan, and Departments of Chemistry and Medicinal Chemistry, Purdue University, West Lafayette, Indiana 47907

Received August 26, 2009

Reliable and robust prediction of the binding affinity for drug molecules continues to be a daunting challenge. We simulated the binding interactions and free energy of binding of nine protease inhibitors (PIs) with wild-type and various mutant proteases by performing GBSA simulations in which each PI's partial charge was determined by quantum mechanics (QM) and the partial charge accounts for the polarization induced by the protease environment. We employed a hybrid solvation model that retains selected explicit water molecules in the protein with surface-generalized Born (SGB) implicit solvent. We examined the correlation of the free energy with the antiviral potency of PIs with regard to amino acid substitutions in protease. The GBSA free energy thus simulated showed strong correlations ($r > 0.75$) with antiviral $IC_{50}$ values of PIs when amino acid substitutions were present in the protease active site. We also simulated the binding free energy of PIs with P2-bis-tetrahydrofuranylurethane (bis-THF) or related cores, utilizing a bis-THF-containing protease crystal structure as a template. The free energy showed a strong correlation ($r = 0.93$) with experimentally determined anti-HIV-1 potency. The present data suggest that the presence of selected explicit water in protein and protein polarization-induced quantum charges for the inhibitor, compared to lack of explicit water and a static force-field-based charge model, can serve as an improved lead optimization tool and warrants further exploration.

## INTRODUCTION

Virtual screening has been successful in the discovery of certain novel inhibitors, and a number of these inhibitors have advanced to clinical trials.[1] When the structure of a target protein is available, virtual screening involves docking potential inhibitors against the protein and ranking the inhibitors by their predicted affinity using a scoring function. Molecular mechanics Poisson–Boltzmann surface area (MM-PBSA) or molecular mechanics generalized Born surface area (MM-GBSA) have been used in some instances in the postprocessing and reranking of results from molecular docking.[2] Of note, docking and scoring have currently been an integral part of drug discovery efforts and produced documented successes; however, there is an urgent need for improvement of the accuracy of docking and scoring results.[3] With this regard, Clark described four areas of improvement, i.e., better scoring functions, treatment of protein flexibility, treatment of water molecules, and improved technology for data analysis of virtual screening results.[1] The scoring functions fail if they do not properly account for solvation, entropy, or polarizability.[1,4]

Water molecules form polar interactions with both proteins and ligands, fill empty spaces in cavities, and serve as an important component of molecular recognition. Lu et al. analyzed water molecules present at the interfaces of 392 X-ray crystal structures of protein–ligand complexes and reported high correlations between the polar van der Waals surface area of ligands and the number of ligand-bound water molecules in the crystal structures.[5] In some instances, as many as 21 water molecules are bound to a ligand, with the average being 4.6.[5] Despite their importance, the treatment of water molecules in docking calculations have not been widespread because of methodological limitations and poor understanding of how many and which water molecules are to be included in the simulation. By sampling multiple water positions during docking, Huang and Shoichet recently assessed the ligand enrichment against 24 targets.[6] Inclusion of water molecules increased enrichment against 12 targets while remaining largely unaffected for the others.[6] Fornabaio et al. reported that waters play a significant role in the energetics of binding and performed a hydropathic analysis of HIV-1 protease complexes.[7] They reported a significant improvement of the correlation between their HINT free energy scores and experimentally determined binding constants when appropriate bridging water molecules were taken into account.[7]

Most of the studies measure the accuracy of scoring functions by their ability to correctly rank the activity of a congeneric set of ligands. The prediction of activity of a ligand against mutant proteins is equally important in light of drug resistance in several diseases including acquired immune deficiency syndrome (AIDS) and cancers. In the

* Corresponding author address: 10 Center Drive, Room 5A11-MSC 1868, Bethesda, MD 20892-1868; phone: 301-496-9238; fax: 301-402-0709; e-mail, hmitsuya@helix.nih.gov.
[†] National Institutes of Health.
[‡] Kumamoto University Graduate School of Medical and Pharmaceutical Sciences.
[§] Purdue University.

10.1021/ci900320p CCC: $40.75 
Published on Web 11/24/2009

present study, we focus on the resistance mutations of HIV-1 protease. HIV-1 protease acquires amino acid substitutions under the selection pressure of protease inhibitors (PIs), rendering HIV-1 resistant to such PIs.[8] For example, an Asp30Asn (D30N) substitution causes resistance against nelfinavir. Some amino acid substitutions, while being initially selected under drug pressure against one inhibitor, confer on HIV-1 cross-resistance against other inhibitors.[8] One example of such a substitution is M46I, which is a primary indinavir-resistance-associated substitution, but M46I-containing HIV-1 is resistant to other inhibitors such as ritonavir, nelfinavir, and atazanavir.[9] Analysis of the crystal structures of interactions of PIs with mutant proteases have shown that a number of drug resistance-associated mutations, such as G48V, V82A, and I84V, occur in the catalytically active site of protease.[10−12] Analyses of crystal structures of mutant proteases have revealed that there are, in general, no major conformational changes to the backbone conformation in such proteases, and the changes in binding interactions from the wild-type may involve different polar interactions with a mutant side chain(s) or loss of favorable van der Waals contacts.[13−15] Structural interactions, which are sometimes able to provide a rational explanation of the mechanism of resistance, are not able to predict a priori, for example, whether V82A causes a higher resistance for ritonavir compared to DRV. More reliable predictions of the potency of inhibitors against protease with drug-resistant mutations would be of use in the design of novel and more potent inhibitors.

The free energy of binding of ligands to proteins can be simulated by methods such as free energy perturbation and linear interaction energy (LIE) approximation.[16,17] LIE is a semiempirical method and based on a linear approximation of polar and nonpolar free energy contributions from molecular dynamics simulation averages.[16] The LIE method has recently been used in calculating the binding free energy of *N*-sulphonyl-glutamic acid inhibitors to MurD ligase and in probing the DNA replication fidelity.[18,19] In the current study we simulated the binding free energies of nine protease inhibitors against wild-type ($PRO^{WT}$) and mutant proteases ($PRO^{MT}$) with standard and hybrid GBSA protocols. While a number of water molecules are present in the X-ray crystal structures of protease−inhibitor complexes, a water molecule that mediates hydrogen-bond interactions of the protease inhibitors with Ile50 and Ile50′ in the flap is common across several different inhibitor−protease complexes and present in the complexes for eight FDA-approved PIs. In this work, we explicitly incorporated water molecule bridging hydrogen bonds with the protease flap. For inhibitors nelfinavir and atazanavir, two additional water molecules that mediate hydrogen bonds between these inhibitors and other protease residues were also explicitly included. We compared the GBSA free energy of binding obtained from simulations with selected explicit water molecules in implicit solvation (a hybrid solvation model) with free energies that did not have the water molecule explicitly present. Furthermore, in the simulations, the inhibitor atoms had either force-field-derived fixed partial charges or quantum mechanics-based partial charges that accounted for the polarization induced by the surrounding protein environment (a hybrid charge model). We also analyzed the correlation of the GBSA free energies obtained by the simulations with antiviral potency data ($IC_{50}$ values). Our current data suggest that selective inclusion of explicit water molecule(s) and protein polarization effects may improve the robustness of GBSA free energy simulations and aid the design of inhibitors that are potent against both wild-type and multidrug-resistant HIV-1 variants.

## METHODS

**Crystal Structures Used as Starting Templates.** We explored various wild-type protease crystal structures from the Protein Data Bank as starting templates for docking and subsequent free energy simulations. For convenience of protein expression and crystallization, some of the structures deposited in the Protein Data Bank as wild-type structures have several mutations such as Q7K, K14R, R41K, L63P, and I64V that are distant from the inhibitor binding site.[15,20,21] These nonactive site mutations may not drastically alter the conformation of the protease and its interactions with inhibitors compared to a pristine wild-type protease of $HIV\text{-}1_{LAI}$ or $HIV\text{-}1_{NL4\text{-}3}$. While one nonactive site mutant, depending on the residue and location, may not necessarily affect the binding affinity comparisons, crystal structures with four or five nonactive site mutations are unsuitable to be used for free energy simulations, especially when comparing the simulation data with antiviral potency against wild-type HIV-1. We used 2FDE, obtained from the Protein Data Bank, as the starting template for docking against darunavir (DRV), amprenavir (APV), GRL-98065, GRL-02031, and GRL-06579. 2FDE is a cocrystal of brecanavir and $HIV\text{-}1_{LAI}$ wild-type protease, and brecanavir (BCV) has a bis-THF ligand as a core.[22] The PDB IDs of the crystal structures used for our simulations of the other inhibitors are as follows: 1HXB[23] for saquinavir (SQV); 2O4P[24] for TPV; 1OHR[25] for nelfinavir (NFV); 1MUI[26] for lopinavir (LPV), and 2AQU[27] for atazanavir (AZV). Waters were not modeled in the crystal structure of LPV[26] but were present in all other structures.

Our goal was to explore the prediction of free energy of binding once a correct binding mode was obtained. In the present study, we demonstrate that the correct binding mode was reliably obtained when a ligand was docked against a protease structure obtained with a similar core. To decrease uncertainty arising due to cross docking of ligands to different proteases, we docked ligands against the native protease crystal or against a protease structure obtained with a similar core. It is important to keep in mind that protease side chains may undergo subtle conformational changes to accommodate protease inhibitors of different shapes and sizes (the molecular weights of the PIs in the current study range from 506 to 705), and these changes might be difficult to capture by simple minimization following ligand docking to non-native crystal structures.

**Docking.** The interactions of protease inhibitors with wild-type HIV-1 protease were examined using computational structural modeling and molecular docking. Besides accounting for the conformational flexibility of the inhibitor, the polarization induced in the inhibitor by the protease was taken into consideration by employing polarizable quantum charges in the docking computations. The use of polarizable quantum charges has recently been shown to substantially improve the prediction of protein−ligand complex structures.[28] The QM-polarized ligand docking protocol utilizing Glide version 4.5, QSite version 4.5, Jaguar version 7.0, and

Maestro version 8.5 (Schrödinger, LLC, New York, NY 2007) was used as described below. The crystal coordinates described above were obtained from the Protein Data Bank (http://www.rcsb.org/) and used as starting templates. Hydrogens were optimized with constraints on the heavy atoms. The crystal water that mediates the interactions between protease inhibitors and the protease flap was retained, and all other crystal waters were deleted. Close interactions in the protease were annealed, and the docking grid was setup. Polarizable ligand charges were determined at the B3LYP/6-31G* level. The extra-precision mode of Glide,[29,30] which has a higher penalty for unphysical interactions, was used. For each docking simulation, up to five final poses were retained and compared with available X-ray structures to verify that the conformations were reasonable. It was particularly important that the correct ring conformations were obtained during docking. LPV produced ring conformations that were different than the conformations obtained from crystal complexes in some docking solutions, and such conformations were discarded for the subsequent GBSA simulations.

**GBSA Scoring Simulations.** The general principle of a GBSA model has been described before. The free energy of binding, $\Delta G_{bind}$ is calculated as[2]

$$\Delta G_{bind} = \Delta E + \Delta G_{solv} + \Delta G_{SA}$$

$$\Delta E = E_{complex} - E_{protein} - E_{ligand}$$

where $E_{complex}$, $E_{protein}$, and $E_{ligand}$ are the minimized energies of the protease−inhibitor complex, protease, and inhibitor, respectively.

$$\Delta G_{solv} = G_{solv(complex)} - G_{solv(protein)} - G_{solv(ligand)}$$

where $G_{solv(complex)}$, $G_{solv(protein)}$, and $G_{solv(ligand)}$ are the solvation free energies of the complex, protein, and inhibitor, respectively.

$$\Delta G_{SA} = G_{SA(complex)} - G_{SA(protein)} - G_{SA(ligand)}$$

where $G_{SA(complex)}$, $G_{SA(protein)}$, and $G_{SA(ligand)}$ are the surface area energies for the complex, protease, and inhibitor, respectively. The simulations were carried out using the GBSA continuum model[31] in Prime, version 2.0 (Schrödinger, LLC, New York, NY, 2008). Prime uses a surface-generalized Born (SGB) model employing a Gaussian surface instead of a van der Waals surface for better representation of the solvent-accessible surface area.[31]

GBSA simulations were carried out for the protease−ligand complex structures obtained by molecular docking. The simulations were carried out in four different scenarios. (i) No water molecules were retained in the protease and ligand atoms have fixed charges based on the OPLS force field. This is the standard MM-GBSA simulation carried out in implicit solvation. The change in free energy obtained is denoted by $\Delta G_{mm}$, and the correlation coefficients are denoted by $r_{mm}$. (ii) No water molecules were retained in the protease and the ligand has protein-polarized QM charges at the B3LYP/6-31G* level. The protein-polarized charge on the ligand is determined from the docked complex and used while computing $E_{complex}$, $G_{solv(complex)}$, and $G_{SA(complex)}$ as well as for $E_{ligand}$, $G_{solv(ligand)}$, and $G_{SA(ligand)}$. The change in free energy obtained is denoted by $\Delta G_{qm}$, and the correlation coefficients are denoted by $r_{qm}$. (iii) The bridging water molecule mediating the hydrogen-bond interactions of inhibitors DRV, GRL-98065, APV, GRL-02031, GRL-06579, NFV, SQV, and AZV with Ile50 and Ile50′ in the flap was explicitly retained. This is a hybrid solvation model since implicit GBSA solvation terms for the whole system were used. For tipranavir (TPV), GBSA with the hybrid solvation model was performed by retaining a water molecule that bridges hydrogen-bond interactions with Gly48 of one monomer of the protease. NFV and AZV were observed to have two additional bridging water molecules, and additional calculations in the presence of three explicit water molecules were performed for NFV and AZV. In the hybrid solvation model, the inhibitors either had MM charges (change in free energy and correlation coefficient denoted by $\Delta G_{mm/wat}$ and $r_{mm/wat}$, respectively) or (iv) protein-polarized QM (B3LYP/6-31G*) charges (change in free energy and correlation coefficient denoted by $\Delta G_{qm/wat}$ and $r_{qm/wat}$, respectively). In all simulations, the protease has OPLS charges. The strain energies of the ligands were taken into account.

**Antiviral Agents.** DRV, GRL-98065, and GRL-02031 were synthesized as described previously.[32−35] SQV and ritonavir (RTV) were kindly provided by Roche Products Ltd. (Welwyn Garden City, United Kingdom) and Abbott Laboratories (Abbott Park, IL), respectively. APV was a kind gift from Glaxo-Wellcome, Research Triangle Park, NC. NFV and indinavir (IDV) were kindly provided by Japan Energy Inc., Tokyo, Japan. LPV was synthesized by previously published methods.[36] AZV was a kind gift from Bristol-Myers Squibb (New York, NY). TPV was obtained through the AIDS Research and Reference Reagent Program, Division of AIDS, NIAID, National Institutes of Health.

**Generation of Recombinant HIV-1 Clones.** To generate HIV-1 clones carrying desired mutations, site-directed mutagenesis using the QuikChange Site-Directed Mutagenesis Kit (Stratagene, La Jolla, CA) was performed, and the mutation-containing genomic fragments were introduced to pHIV-$1_{NLSma}$, as previously described.[35,37] Determination of the nucleotide sequences of plasmids confirmed that each clone had the desired mutations but no unintended mutations. Each recombinant plasmid was transfected into 293T cells using Lipofectoamine 2000 Transfection Reagent (Invitrogen, Carlsbad, CA), and thus generated infectious virions were harvested 48 h after transfection and stored at −80 °C until use. HIV-1 carrying D30N substitution ($HIV^{D30N}$) was generated since residue-30 is in the active site (Figure 1) and the D30N substitution is known to cause primary drug resistance against the FDA-approved protease inhibitor NFV.[38] $HIV^{I50V}$ was generated since Ile50 is in the flap region (Figure 1) and interacts with various PIs through a bridging water molecule.[39] The I50V mutation has been associated with resistance to APV, LPV, and RTV.[40] $HIV^{V82I/I85V}$ was also generated since Val82 is located in the active site and its substitution to Ile is associated with HIV-1 resistance to most PIs, presumably due to the expansion of the active site and loss of favorable van der Waals contact.[15,20,40,41] We recently reported the emergence of I85V as a resistant mutation against a PI, GRL-98065, and chose to study the combined effect of V82A/I85V.[32] HIV-1-infected patients who failed to respond to PI-containing regimens often have HIV-1 variants carrying both active site

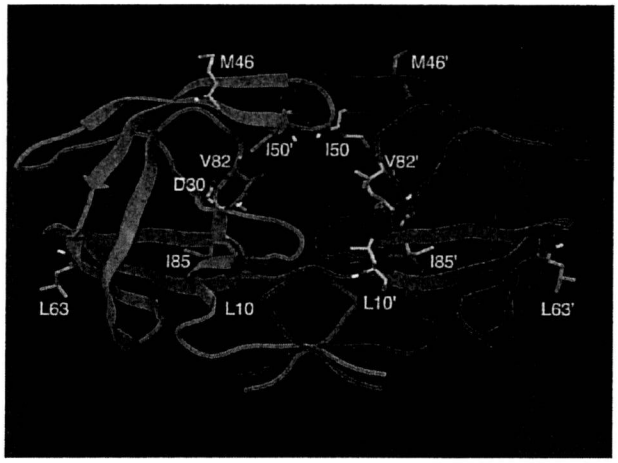


**Figure 1.** Structure of dimerized HIV-1 protease. The monomer subunit is shown in a red or green ribbon. The locations of the mutant residue positions are indicated. Only polar hydrogens are shown, and the following atom colors are used in this and all subsequent figures: C, gray; H, white; O, red; N, blue; S, yellow.

and nonactive site mutations in protease, and we chose to explore such clinical HIV-1 isolates, $HIV^{2840}$ and $HIV^{2841}$. The former contained L10R, M46I, L63P, V82T, and I84V substitutions, while the latter contained M46I, L63P, V82T, and I84V substitutions.

**Drug Susceptibility Assay.** To determine the drug susceptibilities of certain laboratory HIV-1 strains, MT-4 cells were employed as target cells, as described previously,[37] with minor modifications. In brief, MT-4 cells ($10^5$/mL) were exposed to 100 $TCID_{50}$s of drug-resistant HIV-1 strains in the presence or absence of various concentrations of drugs and incubated at 37 °C. On day 7 of culture, the supernatants were harvested and the amounts of the p24 Gag protein were determined by using a fully automated chemiluminescent enzyme immunoassay system (Lumipulse F; Fujirebio Inc., Tokyo, Japan).[42] The drug concentrations that suppressed the production of p24 Gag protein by 50% ($IC_{50}$) were determined by comparison of the amount of p24 Gag protein produced in drug-treated cell cultures with the level of p24 Gag protein produced in a drug-free control cell culture. All assays were performed in duplicate or triplicate on more than three different occasions, and the data are shown as means ± 1 SD.

## RESULTS

**Analysis of Water Molecules in Protease Crystal Structures.** Since the number of ligand-bound water molecules in high-resolution crystal structures varies widely,[5] we first analyzed the number of water molecules in the five protease−inhibitor crystal structures used in the current study. The total number of water molecules ranged from 51 (protease−NFV complex,[25] PDB ID 1OHR) to 124 (protease−TPV complex,[24] PDB ID 2O4P). Within 4 Å of the bound ligand, the number of water molecules present in the complexes with PDB IDs 1HXB, 2FDE, 1OHR, 2O4P, and 2AQU were 3, 5, 5, 10, and 10, respectively. We then analyzed the number of water molecules bridging hydrogen-bond interactions between the protease and the ligands. The water molecule forming tetracoordinated hydrogen-bond interactions with Ile50 and Ile50′ in the flap was the only water molecule interacting with the ligand in the protease complexes of SQV (PDB ID 1HXB), BCV (PDB ID 2FDE), and APV (PDB ID 1HPV[43]). Since this tetracoordinated water molecule is considered an important pharmacophore for protease−inhibitor interactions,[44] it was explicitly included in our docking and GBSA free energy simulations. Three water molecules formed bridging hydrogen-bond interactions in the NFV−protease (PDB ID 1OHR) and AZV−protease (PDB ID 2AQU) complexes (Figure 2c and 2q), and simulations were carried out with both one and three bridging water molecules explicitly present for these inhibitors. TPV directly formed hydrogen bonding with Ile50 and Ile50′, and a water molecule bridged hydrogen bonding with Gly48 in the flap (Figure 2g)[24,45,46] and was explicitly included in the simulations. Simulations involving LPV did not include any crystal waters since none were present in the native LPV−protease complex.[26]

**Determination of the Susceptibility of Recombinant Infectious HIV-1 Clones Carrying Amino Acid Substitutions to PIs in Vitro.** We determined the susceptibility of six recombinant infectious HIV-1 clones to each of the PIs that were chosen in the present study: 7 clinically available PIs (SQV, NFV, APV, TPV, DRV, and AZV) and 2 experimental PIs (GRL-02031 and GRL-98065) in the HIV-1 p24 Gag production inhibition assay, as previously described.[35,37] As illustrated in Table 1, most of the recombinant clones showed reduced susceptibility to the PIs examined by up to 16.5-fold. However, it was also noted that $HIV^{D30N}$ and $HIV^{2841}$ had increased susceptibility to certain PIs. The increased susceptibility of $HIV_{D30N}$ to TPV with 33.3-fold was notable, although $HIV^{D30N}$ was also less susceptible to SQV, LPV, and NFV (Table 1). Both $HIV^{I50V}$ and $HIV^{2840}$ were also less susceptible to most of the PIs (Table 1).

**Binding Interactions with Wild-Type and D30N Mutant Protease.** We next determined and analyzed the binding modes of nine different PIs with $PRO^{WT}$ and a protease with an amino acid substitution at position 30 from an aspartic acid to asparagine ($PRO^{D30N}$). SQV has four hydrogen-bond interactions with Asp29 and Asp30 in the S2 site of the wild-type protease but has no hydrogen bonds with Asp29′ or Asp30′ in the S2′ site (Figure 2a). When protease acquires the D30N mutation, SQV loses two hydrogen bonds with Asp29 and Asp30 and does not form any new and compensating hydrogen bonds with other protease residues (Figure 2b). Comparison of the antiviral data of SQV shown in Table 1 indicates that there was a 3.9-fold decrease in antiviral potency with the D30N mutation. It is possible that the decrease of antiviral potency of SQV for D30N mutant is due to the loss of hydrogen bonds with residues 29 and 30 for the mutant. Examining the hydrogen bonds in the S2 site for NFV against $PRO^{WT}$ and $PRO^{D30N}$ mutant protease (Figure 2c and 2d), one observes that NFV has more hydrogen bonds with Asn30 of $PRO^{D30N}$ compared to Asp30 of $PRO^{WT}$. An X-ray crystal structure has also demonstrated that NFV has a larger number of hydrogen bonds with $PRO^{D30N}$ than with $PRO^{WT}$.[11]

However, D30N is a major amino acid substitution[38] associated with NFV resistance of HIV-1, and $HIV^{D30N}$ showed a 5.3-fold increase in $IC_{50}$ values in antiviral assays

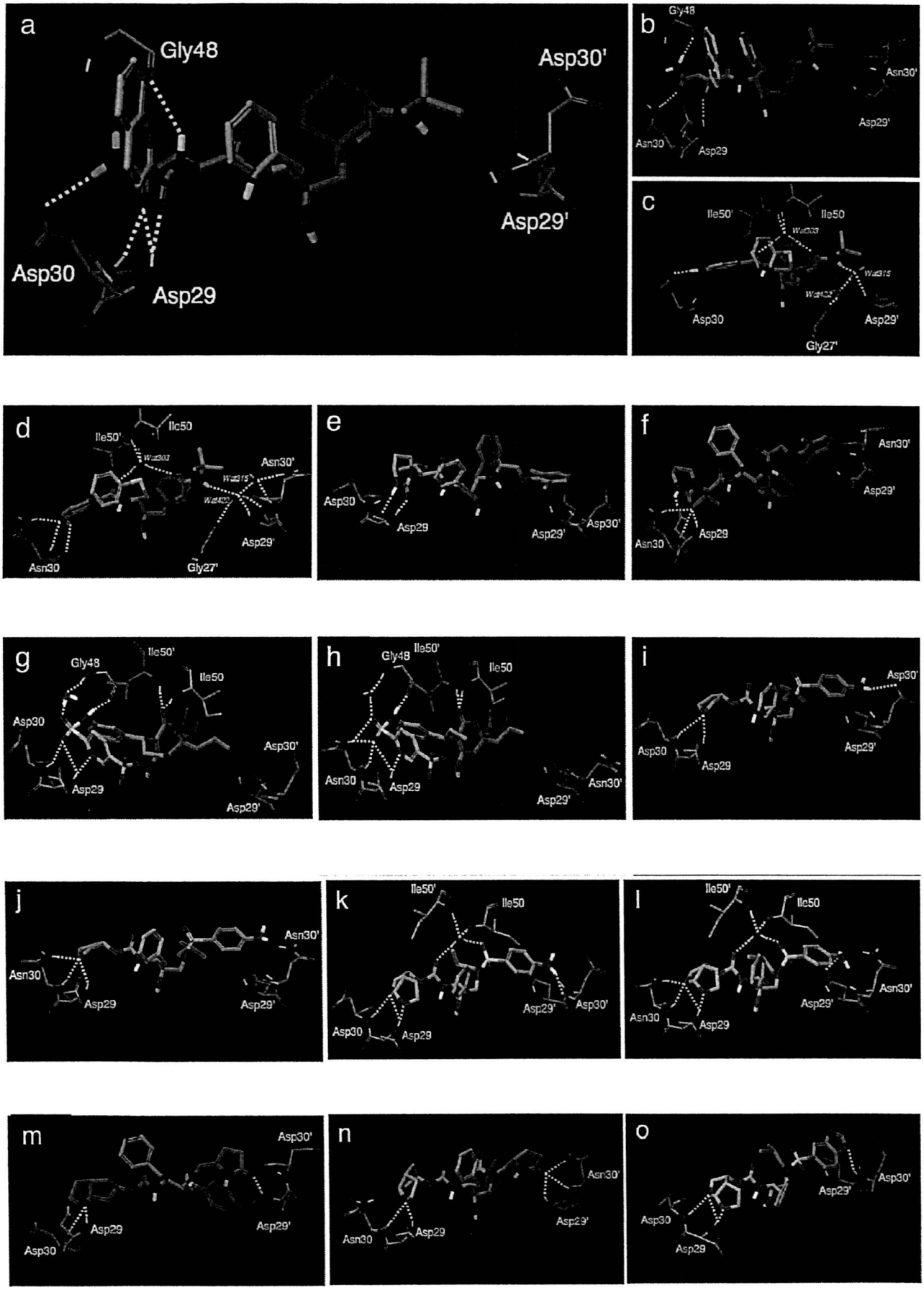
a
Gly48
Asp30'
Asp29'
Asp30
Asp29
b
Gly48
Asn30'
Asp29'
Asn30
Asp29
c
Ile50'
Ile50
Asp30
Asp29'
Gly27'
d
Ile50'
Ile50
Asn30'
Asp29'
Asn30
Gly27'
e
Asp30
Asp29
Asp29'
Asp30'
f
Asn30'
Asp29'
Asn30
Asp29
g
Gly48
Ile50'
Ile50
Asp30
Asp30'
Asp29
Asp29'
h
Gly48
Ile50'
Ile50
Asn30
Asp29
Asp29'
Asn30'
i
Asp30'
Asp30
Asp29
Asp29'
j
Asn30'
Asn30
Asp29
Asp29'
k
Ile50'
Ile50
Asp29'
Asp30'
Asp30
Asp29
l
Ile50'
Ile50
Asn30'
Asp29'
Asn30
Asp29
m
Asp30'
Asp29
Asp29'
Asp30
n
Asn30'
Asn30
Asp29
Asp29'
o
Asp30'
Asp29'
Asp30
Asp29

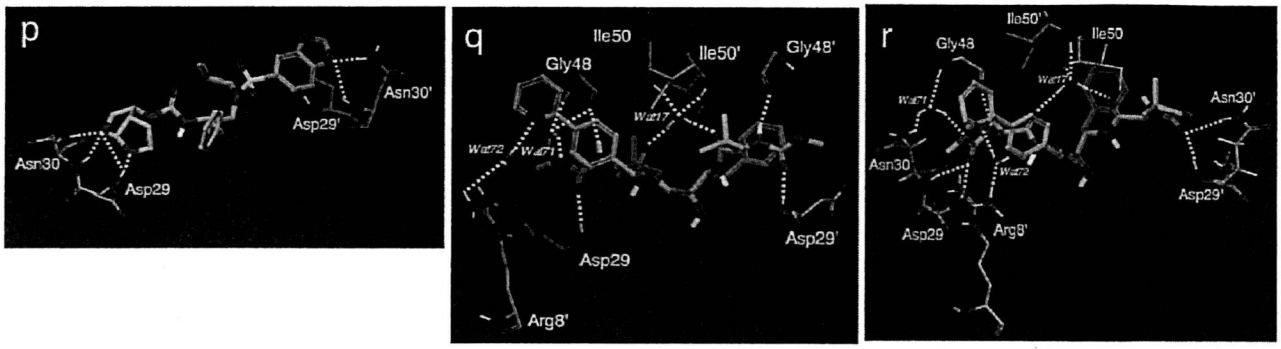


**Figure 2.** Interactions of protease inhibitors with wild-type and D30N mutant protease. Interactions of SQV with (a) wild-type ($PRO^{WT}$) and (b) D30N-containing mutant protease ($PRO^{D30N}$) are shown. SQV has hydrogen-bond interactions (dotted yellow lines) only in the S2 site but no such interactions in the S2′ site. The hydrogen bonds of SQV with the mediating water molecule, Asp25, Asp25′, and Gly27, are present but not shown. Hydrogen-bond interactions of NFV with (c) $PRO^{WT}$ and (d) $PRO^{D30N}$. The bridging water-303 has hydrogen bonds with Ile50 and Ile50′, water-315 hydrogen bonds with Asp29′, and water-422 hydrogen bonds with Gly27′. Simulations were carried out for NFV with these three waters molecules explicitly present, with one of the bridging water molecules and without any explicit water molecule. Nefinavir has more hydrogen bonds with residues 29 and 30 in $PRO^{D30N}$ even though it has a lower antiviral potency against HIV-$1^{D30N}$. Hydrogen bonds of LPV with (e) $PRO^{WT}$ and (f) $PRO^{D30N}$. LPV has more hydrogen-bond interactions with the S2 site for the mutant than it has for the $PRO^{WT}$. The crystal structure for LPV 1MUI (PDB ID) does not have waters. Hydrogen-bond interaction of TPV with (g) $PRO^{WT}$ and (h) $PRO^{D30N}$. Unlike other inhibitors in this study, TPV directly hydrogen bonds with Ile50 and Ile50′ but a bridging water molecule hydrogen bonds with Gly48 in the flap. Interactions of APV with (i) $PRO^{WT}$ and (j) $PRO^{D30N}$ are shown. In the S2 site of the protease, the THF ligand of APV has an additional hydrogen bond with Asn30 ($PRO^{MT}$) compared to Asp30 ($PRO^{WT}$). In the S2′ site, the aniline nitrogen of APV has a hydrogen bond with the side chain of Asp30 ($PRO^{WT}$) and the hydrogen bond is lost for the Asn30 mutant. Structural interaction of DRV with (k) $PRO^{WT}$ and (l) $PRO^{D30N}$ are shown. The bis-THF ligand of DRV has more hydrogen-bond interactions with $PRO^{D30N}$ compared to the $PRO^{WT}$. The water molecule mediating hydrogen bonds between the inhibitor and Ile50 and Ile50′ in the flap is shown. The water molecule is present in docking and free energy simulations of APV, GRL-98065, GRL-02031, and SQV but is not shown. Hydrogen-bond interactions of GRL-02031 with (m) $PRO^{WT}$ and (n) $PRO^{D30N}$ are shown. (o) Hydrogen-bond interactions of GRL-98065 with wild-type protease are shown. The bis-THF ligand of GRL-98065 has hydrogen-bond interactions with backbone atoms of Asp29 and Asp30 in the S2 site and with Asp30′ in S2′. (p) Besides maintaining the backbone hydrogen bonds with Asp29 and residue-30 and -30′ of $PRO^{D30N}$, GRL-98065 forms additional hydrogen bonds with the side chains of Asn30 and Asn30′. Hydrogen-bond interactions of AZV with (q) $PRO^{WT}$ and (r) $PRO^{D30N}$.

**Table 1.** Antiviral $IC_{50}$ Values ($\mu$M) of Protease Inhibitors against Wild-Type and Mutant Protease

| inhibitor | $HIV^{WT}$ $IC_{50}$ ($\mu$M) | $HIV^{D30N}$ $IC_{50}$ ($\mu$M) | $HIV^{I50V}$ $IC_{50}$ ($\mu$M) | $HIV^{V82I/I85V}$ $IC_{50}$ ($\mu$M) | $HIV^{2840}$ $IC_{50}$ ($\mu$M) | $HIV^{2841}$ $IC_{50}$ ($\mu$M) |
|---|---|---|---|---|---|---|
| saquinavir | 0.008 ± 0.003[a] | 0.031 ± 0.005 (3.9)[b] | 0.034 ± 0.001 (3.9) | 0.023 ± 0.01 (2.9) | 0.015 ± 0.009 (1.9) | 0.004 ± 0.0004 (0.5) |
| nelfinavir | 0.018 ± 0.002 | 0.096 ± 0.005 (5.3) | 0.11 ± 0.08 (6.1) | 0.083 ± 0.071 (4.6) | 0.22 ± 0.05 (12.4) | 0.031 ± 0.005 (1.7) |
| lopinavir | 0.018 ± 0.001 | 0.055 ± 0.011 (3.1) | 0.21 ± 0.14 (11.7) | 0.037 ± 0.007 (2.1) | 0.30 ± 0.009 (16.5) | 0.048 ± 0.009 (2.7) |
| amprenavir | 0.028 ± 0.007 | 0.0066 ± 0.0049 (0.2) | 0.16 ± 0.13 (5.7) | 0.058 ± 0.024 (2.1) | 0.083 ± 0.018 (3.0) | 0.038 ± 0.003 (1.4) |
| tipranavir | 0.15 ± 0.05 | 0.0047 ± 0.0002 (0.03) | 0.34 ± 0.03 (2.3) | 0.28 ± 0.003 (1.9) | 0.32 ± 0.01 (2.2) | 0.12 ± 0.05 (0.8) |
| darunavir | 0.003 ± 0.0007 | 0.0015 ± 0.0013 (0.5) | 0.014 ± 0.012 (4.7) | 0.0057 ± 0.0024 (1.9) | 0.0033 ± 0.0001 (1.1) | 0.0018 ± 0.0008 (0.6) |
| GRL-02031 | 0.02 ± 0.008 | 0.0087 ± 0.0067 (0.4) | 0.014 ± 0.001 (0.7) | 0.036 ± 0.002 (1.8) | 0.033 ± 0.0009 (1.7) | 0.012 ± 0.001 (0.6) |
| GRL-98065 | 0.0003 ± 0.00006 | 0.00055 ± 0.00035 (1.8) | 0.0018 ± 0.001 (6.0) | 0.0018 ± 0.0007 (6.0) | 0.0004 ± 0.0001 (1.3) | 0.00015 ± 0.00007 (0.5) |
| atazanavir | 0.004 ± 0.0004 | 0.0016 ± 0.0008 (0.4) | 0.0019 ± 0.001 (0.5) | 0.0015 ± 0.0001 (0.4) | 0.0086 ± 0.0041 (2.2) | 0.003 ± 0.001 (0.8) |

[a] The $IC_{50}$ values shown represent means ± 1 SD of assays conducted in duplicate or triplicate on more than three different occasions for the study. [b] The fold change in activity of the mutants from the wild-type $IC_{50}$ are shown within brackets.

(Table 1). Examining the structural interactions of LPV and TPV against $PRO^{WT}$ and $PRO^{D30N}$ mutants (Figure 2e–h), we observed that both inhibitors have more hydrogen bonds with residues 29 and 30 of $PRO^{D30N}$ than they have for those of $PRO^{WT}$. Antiviral data show that while LPV has a 3.1-fold increase in $IC_{50}$, $HIV^{D30N}$ was about 30 times more sensitive to TPV (Table 1). Comparison of the structural interactions of DRV, TPV, GRL-02031, and GRL-98065 with $PRO^{WT}$ and $PRO^{D30N}$ (Figure 2k–p) revealed that all of them have more hydrogen-bond interactions with $PRO^{D30N}$. APV, which is 5-fold more potent against $HIV^{D30N}$ (Table 1), has three hydrogen bonds with Asp29, Asp30, and Asp30′ for $PRO^{WT}$ and forms three hydrogen bonds with Asp29 and Asn30 for $PRO^{D30N}$ in structural models (Figure 2i and 2j). Thus, it is clear that while the number of hydrogen bonds may provide an intuitive understanding of binding and/or antiviral potency, it may not always explain why certain PIs show a decrease in antiviral potency with D30N substitution while other PIs show an increase.

**Free Energy Changes in Complexes with the D30N Mutation Determined by GBSA Simulations.** Since the number of hydrogen bonds between PIs and protease does not always help predict the potency of PIs as discussed above, we examined the free energies under four different simulation conditions: with and without explicit water(s) and with QM or with MM charges on the inhibitor (Table 2, Supporting Information Tables S1 and S2). It was assumed that an increase in the change of free energy of binding ($\Delta\Delta G$ more positive) is to be expected for a decrease in antiviral activity and vice versa. With the D30N mutation in $PRO^{D30N}$, SQV showed a reduction in antiviral activity by 3.9-fold. With the bridging water and QM charges on SQV, the free energy change ($\Delta\Delta G_{qm/wat}$) of the SQV–protease complex increased by 4 kcal/mol for the D30N mutation (Table 2). $HIV^{D30N}$